Algal Research 69 (2023) 102934

Contents lists available at ScienceDirect

Algal Research

journal homepage: www.elsevier.com/locate/algal

Light and carbon limited photosynthesis of *Chlorella sorokiniana*

Hiroki Yoshida, Sabine van Oossanen, Maria J. Barbosa, Marcel Janssen *

Bioprocess Engineering, AlgaePARC, Wageningen University and Research, P.O. Box 16, 6700 AA Wageningen, the Netherlands

ARTICLE INFO

Keywords:
Carbon response
Light response
Photorespiration
Carbon concentrating mechanism
CO_2-based photosynthesis monitor

ABSTRACT

Carbon dioxide (CO_2) and light are essential for high photosynthetic rates of microalgal cultures. Microalgal photosynthetic behavior at low CO_2 concentrations has not been revealed yet at the same level of detail as leaf photosynthesis. In the present study, we investigated the short-term photosynthetic response of suspended *Chlorella sorokiniana* to limiting light intensity and CO_2 concentration. We used a novel CO_2-based photosynthesis monitor originating from leaf research but equipped with an aquatic chamber sparged with CO_2 enriched air. Photosynthesis was measured by employing a steady-state CO_2 mass balance over the chamber. Light and carbon response curves were determined under constant pH, temperature, dissolved oxygen, light intensity or dissolved carbon dioxide. We determined the volumetric mass transfer coefficient of the aquatic chamber to accurately convert gaseous CO_2 partial pressure into aqueous CO_2 concentration to evaluate the CO_2 response measurements.

Light response measurements on dilute algal cultures revealed a high photosynthetic capacity on a time scale of minutes which by far exceeded the average CO_2 uptake on a time scale of hours (cell growth). Light response measurements with dense and fully absorbing cultures provided accurate insight into the response of microalgal mass culture to changing incident irradiance, including the efficiency of photosynthesis of the algal culture as a whole. CO_2 response measurements demonstrated severe CO_2 limitation at dissolved CO_2 levels of $<$20 μM giving a concrete target for optimization of CO2 supply in large-scale cultivation systems. Measurements at a background of either 21 % O_2 (air) or 2 % O_2 indicated the existence of photorespiration in *Chlorella*. Moreover, the magnitude of photorespiration first increased and then decreased again while reduced dissolved CO_2 levels, indicating the activation of a carbon concentrating mechanism at low CO_2. Simultaneous measurement of the quantum yield of PSII linear electron transport (ϕ_{PSII}) and CO_2 uptake revealed the transition of CO_2 limited photosynthesis towards light-limited photosynthesis.

1. Introduction

As represented by the discovery of the reductive pentose phosphate cycle (so-called Calvin–Benson–Bassham (CBB) cycle) using green algae such as *Chlorella* [1], microalgae have been actively employed in plant physiology, especially at the early stage of photosynthesis studies [2]. Plant physiologists revealed fundamental theories on photosynthesis by studying unicellular microalgae [3], including eponymous discoveries such as the Warburg effect [4], the Emerson effect [5,6], and the Kok effect [7]. Nowadays, microalgae additionally attract more attention as sustainable feedstocks for a wide variety of products such as food and feed, bulk or high-value chemicals, and fuels [8–10].

Low availability of carbon dioxide (CO_2) or light limits photosynthesis. Algal photosynthetic behavior at low CO_2 concentrations, however, has not been revealed at the same level of detail as compared to leaf photosynthesis. Therefore, excessive amounts of CO_2 are typically supplied to photobioreactors to avoid the CO_2 limitation of photosynthesis, although CO_2 is a major operating cost in microalgal cultivation [11,12]. In fact, a cost analysis revealed that the CO_2 consumption accounted for 71 % of the total cost for raw materials and could make up 30 % of the overall biomass production cost when pure CO_2 gas is used [13]. Lower CO_2 concentrations in the liquid phase of a photobioreactor provide a larger driving force for the transfer of CO_2 from the gas phase to the liquid phase, leading to the reduction of gassing in microalgal mass culture. Moreover, reactor operation at low CO_2 levels and reduced gassing rates will also lead to less CO_2 loss via the off-gas of the system. A detailed insight into CO_2 limitation in algal photosynthesis, therefore, has the potential to reduce the CO_2-related operating cost of a photobioreactor.

In contrast, leaf photosynthetic response to low CO_2 concentrations

* Corresponding author.
E-mail address: marcel.janssen@wur.nl (M. Janssen).

https://doi.org/10.1016/j.algal.2022.102934
Received 9 June 2022; Received in revised form 11 November 2022; Accepted 6 December 2022
Available online 12 December 2022

has been well investigated, especially since the biochemical model for photosynthesis in C_3 plants was proposed by Farquhar, von Caemmerer, and Berry [14]. This so-called Farquhar-von Caemmerer-Berry model or FvCB model has contributed to a wide range of studies in leaf and canopy photosynthesis, from analyzing biochemistry in leaf photosynthesis to predicting CO_2 assimilation rates under different environmental conditions [15–18].

Photosynthetic CO_2 assimilation is catalyzed by ribulose-1,5-bisphosphate carboxylase-oxygenase (RuBisCO) [19]. The competitive oxygenation reaction of RuBisCO reduces the CO_2 assimilation rate (i.e., photorespiration effect) as this reaction leads to the loss of part of the carbon fixed in the CBB cycle [4]. The enzyme affinity for CO_2 and oxygen molecules determines the kinetics of competitive reactions [20]. This photorespiration effect could be more visible at low CO_2 concentrations because the ratio of oxygen molecules to CO_2 molecules becomes higher. To deal with the competitive oxygenation reaction and low RuBisCO's affinity for CO_2, microalgae have adapted to low CO_2 concentrations by a carbon concentrating mechanism (CCM) [21]. A CCM functions to facilitate CO_2 assimilation by enhancing internal CO_2 concentrations when the availability of CO_2 is limited [22]. Active uptake of bicarbonate promotes accumulation of bicarbonate in the cell, and then internal carbonic anhydrase elevates the CO_2 concentration at the active site of RuBisCO by dehydration of accumulated bicarbonate [22].

As Farquhar called a “see-saw” [23], the photosynthesis rate is determined by a relative contribution of the applied light intensity and CO_2 concentration. Despite this relative relationship, most preceding studies on carbon response in an algal culture considered only the carbon-limited photosynthesis for all the examined inorganic carbon concentrations, which would include the light-limited region [24–30]. Most of them applied the typical Monod equation to fit the measured carbon response curves [24,26–28]. However, this simplification obviously ignores the complexity of algal photosynthesis, such as the mitochondrial respiration in the light, the potential existences of the photorespiration effect, a CCM, or light-limited photosynthesis.

A lack of photosynthesis monitors able to meet the complexity of the algal world hinders the development of models that accurately describe algal photosynthesis at low CO_2 concentrations. The most popular short-term photosynthesis monitor is based on the continuous measurement of the oxygen concentration in a liquid phase [31–36]. A dissolved oxygen-based photosynthesis monitor is relatively simple and cheap. On the one hand, this photosynthesis monitor allows for a short measurement because it is based on either a Clark-type oxygen electrode [32,33,35,37] or an optical oxygen sensor [36]. On the other hand, a closed system with photosynthesizing algal culture results in oxygen accumulation, which could cause growth inhibition due to photorespiration and other possible physiological effects of high dissolved oxygen levels [38–40]. Furthermore, a closed system does not allow for accurate control of inorganic carbon concentrations, and the measurement is often implemented with an inorganic carbon concentration well above its saturation level [31,37,41–43]. This characteristic of closed liquid-phase photosynthesis monitors hinders easy access to algal photosynthetic response at low CO_2 concentrations.

Looking back at the development in plant physiology, photosynthesis monitors based on a CO_2 gas exchange system with infrared gas analysis (IRGA) have been providing simple, rapid, and reliable measurements in leaf photosynthesis for years [15,16]. Furthermore, it is worth noting that simultaneous chlorophyll fluorescence measurements with photosynthetic CO_2 exchange measurements have led to the identification of key biochemical and biophysical responses in leaf photosynthesis [16]. The present research proposes using an open gas exchange system with CO_2 IRGA and simultaneous chlorophyll fluorescence measurements in the algal community as a new extensive methodology to measure photosynthesis rates in algae suspension cultures.

One of the drawbacks of CO_2 gas exchange photosynthesis monitors for algal cultures is uncertainty regarding the CO_2 and dissolved inorganic carbon (DIC) concentration in the liquid phase. This characteristic could obstruct a correct plotting of a carbon response curve, namely a photosynthesis rate as a function of a CO_2 (or DIC) concentration in a liquid phase. For instance, Shelp and Canvin [26,27] assumed without justification that the CO_2 concentration in the liquid phase was the same as an equilibrium concentration at a gas-liquid interface. The true concentration, however, must have depended on gassing conditions in their measurements and must have been lower than the equilibrium concentration. In our study, we, therefore, present a determination of the mass transfer coefficient in the aquatic chamber of our photosynthesis monitor by making use of the dynamic response in carbonate chemistry.

The objective of the present study is to investigate the photosynthetic response of suspended *Chlorella sorokiniana* to low CO_2 concentrations. First, we discuss the importance of biomass concentrations in the photosynthetic response of suspended algal culture, addressing our findings in the light response measurements. Then, we examine the influence of oxygen concentration and light intensity on the microalgal carbon response. Lastly, we summarize the complexity of algal photosynthesis observed in the present study for future improvement of algal photosynthetic response models.

2. Materials & methods

2.1. Cultivation of algae sample

Chlorella sorokiniana was cultivated in a flat panel airlift photobioreactor (Algaemist, Technical Development Studio, Wageningen University, the Netherlands) with a working volume of 0.4 L, an optical depth of 14 mm, and an air flow rate of 400 mL min^{-1} [44]. The reactor temperature was maintained at 37 °C, and the pH was controlled at 6.7 with on-demand CO_2 addition. The reactor was operated in a turbidostat mode with the incident light of 916 $\mu mol_{ph}\ m^{-2}\ s^{-1}$ and outgoing light of 3.1 $\mu mol_{ph}\ m^{-2}\ s^{-1}$. M8a medium [44] was used as cultivation medium after setting the pH at 6.7 and adding sodium bicarbonate to obtain a concentration of exactly 1000 μM. On-demand CO_2 addition then resulted in a dissolved CO_2 concentration of 350 μM and a dissolved inorganic carbon (DIC) concentration of 1350 μM at pH 6.7 and 37 °C. The equilibrium gas concentration was 1.35 % *v*/v (Appendix 3 & 4).

2.2. Photosynthesis measurements

2.2.1. Photosynthesis monitor configuration

We used a CO_2 based photosynthesis monitor LI-6800 with an aquatic chamber 6800-18 prototype (diameter 31.75 mm, optical path 25.4 mm) (LI-COR Biosciences, Lincoln, Nebraska, USA) [45]. The LI-6800 is an open gas exchange system with infrared gas analyzers. Photosynthesis measurements are based on the difference in the CO_2 concentration at the inlet gas (C_{gCO_2ref}) and the outlet gas (C_{gCO_2sam}) of the gas exchange system. The LI-6800 is also able to measure chlorophyll fluorescence under a range of light conditions. A series of portable open gas exchange photosynthesis monitors, including LI-6800, with a leaf chamber has been widely utilized for leaf photosynthesis measurements [16].

The gas exchange system is illustrated in Fig. 1. In the combined system, the gas-liquid mass transfer in the aquatic chamber, which is coupled to CO_2 assimilation by suspended algal culture, can be detected as the difference in the CO_2 concentration at the inlet gas (C_{gCO_2ref}) and the outlet gas (C_{gCO_2sam}) of the gas mixer. The following describes the process flow in the system: refer to the original paper from the manufacturer for the details [45]. The inlet gas (subscript ‘ref’) is prepared by drawing ambient air (or chosen gas source) with an air pump and controlling the CO_2 concentration (C_{gCO_2ref}) as well as the water vapor concentration (C_{gH_2Oref}) (Fig. 1). This inlet gas is first fed to a gas mixer with a controlled flow rate (F_g) where it is mixed by a fan with the gas returning from the aquatic chamber (subscript ‘cha’). This mixing event

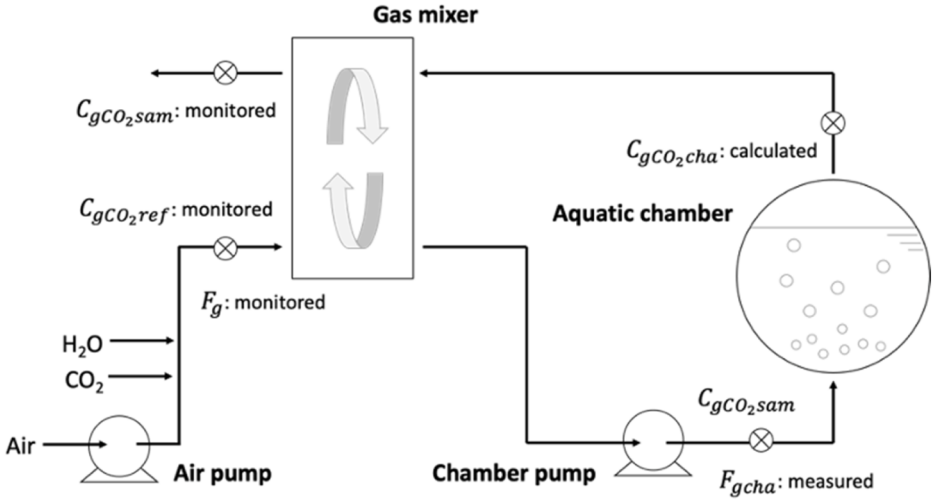

Fig. 1. Schematic drawing of the CO_2 based photosynthesis monitor combined with the aquatic chamber used in this research.

is assumed to be instantaneous (i.e. ideal mixing) and results in the so-called sample gas (subscript 'sam'). Part of the sample gas is drawn by the chamber pump and sparged into the aquatic chamber with the algal suspension to induce intensive gas-liquid contact and gas-liquid mass transfer. The outgoing gas from the chamber is returned to the gas mixer. Surplus sample gas in the gas mixer is purged from the system. The CO_2 concentration of the purged gas (C_{gCO_2sam}), as well as the water vapor concentration at the same point (C_{gH_2Osam}), are continuously monitored. The CO_2 exchange flux (F_{CO_2}) is calculated in the device as the difference in CO_2 concentration at the inlet (C_{gCO_2ref}) and the outlet (C_{gCO_2sam}) of the gas mixer while correcting for the water vapor concentration at both points:

$F_{CO_2} = F_{CO_2} \bullet 10^{-6} \bullet [C_{gCO_2ref} - C_{gCO_2sam} \bullet (10^{-3} - C_{gH_2Oref})/(10^{-3} - C_{gH_2Osam})]$ [45].

The gas flow rate to the chamber (F_{gcha}) was separately determined as per the manufacturer's manual.

2.2.2. Light response measurement

All the light response curves were measured using ambient air and maintaining the CO_2 concentration of 2700 μmol mol^{-1} at the inlet to the gas exchange system (C_{gCO_2ref}). The summary of the controlled parameters is listed in Table 1. The light composition was 50 % blue (475 nm) and 50 % red (625 nm) LED. The temperature of the stainless-steel chamber block (T_{aq}) was maintained between 36.8 and 37.1 °C by circulating water from an external water bath through an integrated heat exchanger. According to the manufacturer's manual, the liquid temperature (T_{liq}) can be considered equal to the chamber block temperature, which was continuously monitored.

Samples were prepared by diluting algal culture from the photobioreactor in steady condition with cultivation medium to reach a biomass concentration of 0.13 g_x L^{-1}. An algal sample of 15 mL was injected into the aquatic chamber and kept in the dark while gassing for approximately 60 min for undiluted samples (or 30 min for diluted samples) to equilibrate the liquid to the applied CO_2 concentration and reach a constant CO_2 exchange flux. After recording the dark condition, the light intensity applied to the chamber was increased stepwise over 11 levels with a 6-min interval. The CO_2 exchange flux and other operating parameters were recorded at the end of each interval. Chlorophyll fluorescence measurements were simultaneously implemented by the LI-6800 Multiphase Flash Fluorometer (LI-COR Biosciences, Lincoln, Nebraska, USA) with the following measuring parameters: the measuring light's modulation rate of 500 Hz (in the dark) or 50 kHz (under actinic light), and the red saturation flash of 8000 μmol_{ph} m^{-2} s^{-1} with the duration of 500 ms.

The above measurement protocol was also applied to undiluted samples taken from the photobioreactor in steady conditions with biomass concentrations ranging between 2.52 and 2.86 g_x L^{-1}.

Table 1
Summary of controlled and measured parameters for light response and carbon response measurements.

Parameters		Unit	Light	Carbon
C_{gCO_2ref}	Controlled	μmol mol^{-1}	2700	0–2700
q_{in}	Controlled	μmol_{ph} m^{-2} s^{-1}	0–2484	415 or 830
Biomass concentration	Measured	g_x L^{-1}	0.13 (diluted)	0.12–0.14
pH	Measured	–	7.1–7.2	7.1–7.3
F_g	Controlled	μmol s^{-1}	300	
F_{gcha}	Determined	μmol s^{-1}	190	
T_{aq}	Controlled	C°	36.8–37.1	
C_{gH_2Oref}	Controlled	mmol mol^{-1}	20	
Light source (LED)	Controlled	–	50 % Red: 50 % Blue	

2.2.3. Carbon response measurement

Two different gas mixtures were used for the inlet gas, ambient air with 21 % oxygen and a gas mixture of air-nitrogen with 2 % oxygen gas from a gas cylinder.

Diluted algal suspensions were prepared as described for the light response measurements aiming for biomass concentrations between 0.12 and 0.14 g_x L^{-1}. During carbon response measurements, 1 mg of carbonic anhydrase was added to the diluted sample. Carbon anhydrase facilitates the otherwise slow hydration of CO_2 when changing the CO_2 concentration. The summary of the controlled parameters is listed in Table 1. As with the light response, a diluted sample of 15 mL was injected into the chamber and kept for about 30 min in the dark and at the CO_2 concentration of 2700 μmol mol^{-1} at the inlet to the gas exchange system (C_{gCO_2ref}). After recording the dark-acclimated condition at the end of the period, the light intensity to algal samples was increased to the target intensity, either 415 or 830 μmol_{ph} m^{-2} s^{-1}, and the starting condition was recorded after approximately 10 min. The CO_2 concentration at the inlet to the gas exchange system (C_{gCO_2ref}) was decreased stepwise from 2700 to 0 μmol mol^{-1} (11 steps in total) with a 6-min interval. All measurements and operating parameters were recorded at the end of each interval.

2.3. Dry weight measurements

The biomass concentration of the algal sample was determined as dry weight by filtration with a Whatman GF/F glass microfiber filter

(diameter 55 mm, pore size 0.7 μm). An empty filter was dried in an oven at 100 °C overnight and weighted as a blank weight after being cooled down in a desiccator. The empty filter was used for filtering 2.5 mL of algal sample and washed with demineralized water. The filter with biomass was then dried and weighed in the same manner. The biomass concentration was determined from technical duplicates using the difference in weight between the empty filter and the filter with biomass.

2.4. Calculations

2.4.1. CO_2 assimilation rate

The areal CO_2 assimilation rate (A_{CO_2}) and the specific CO_2 assimilation rate (q_{CO_2}) were calculated as follows:

$$A_{CO_2} = \frac{F_{CO_2}}{r_{CO_2/x} \bullet A_{cham}} \tag{1}$$

$$q_{CO_2} = \frac{F_{CO_2}}{r_{CO_2/x} \bullet C_x \bullet V_{lcha}} \tag{2}$$

where A_{cham} is the illuminated area in the aquatic chamber, $r_{CO_2/x}$ is the stoichiometry of CO_2 to the biomass in the growth equation, and C_x is the molar biomass concentration, and V_{lcha} is the liquid volume in the chamber. The molar biomass concentration was calculated from the dry weight assuming the molecular weight (M_x) of 24 g mol^{-1} [46].

The stoichiometry of CO_2 to the biomass ($r_{CO_2/x}$, 0.93) was included to reflect that part of the carbon assimilated by algae is supplied from the hydrolyzed urea, as shown in the growth equation (Appendix 1).

2.4.2. Light intensity in the aquatic chamber

The photosynthesis monitor used in this research only records the fluorometer output at the inlet to the chamber (Q_f) and the light intensity at the outlet from the chamber (q_{exit}) (Fig. 2). The latter was continuously measured with an integrated LI-190R quantum sensor (LI-COR Biosciences, Lincoln, Nebraska, USA). Therefore, the calculation for light absorption by algal samples first requires a good estimation of the incoming light intensity to samples (q_{in}) and the outgoing light intensity from samples (q_{out}).

The following describes the estimation method using a light measurement with the quantum sensor at a certain fluorometer output. First, when the fluorometer output (Q_f) was 1000, the light intensity on the front glass was determined as the average value (q_{inave}) through light measurements over the entire front glass. Results are presented in the supporting information (**Supporting Information 1**). The spatial average value along the radius of the glass was used because higher light intensities were observed at the outer radial positions of the glass surface. Then, the conversion factor (f) to estimate the incoming light intensity (q_{in}) from the fluorometer output (Q_f) was introduced as below:

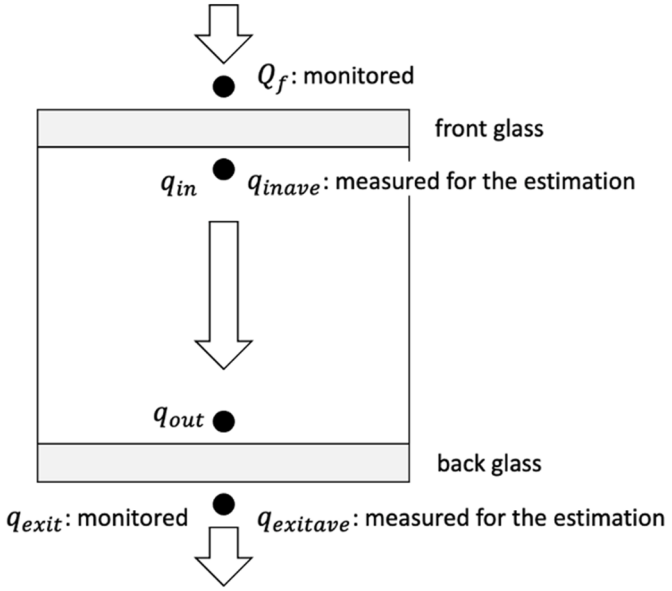

Fig. 2. Schematic drawing of light distribution over the aquatic chamber.

$$f = \frac{q_{in}}{Q_f} = \frac{q_{inave}}{Q_f} = 0.83\ \mu\mathrm{mol_{ph}}\ \mathrm{m^{-2}}\ \mathrm{s^{-1}} \tag{3}$$

As a result, the incoming light intensity on the samples (q_{in}) can now be estimated for any fluorometer output:

$$q_{in} = f \bullet Q_f \tag{4}$$

In order to calculate the outgoing light intensity from samples (q_{out}), the light distribution over the whole back glass was measured (**Supporting Information 1**) with water inside the aquatic chamber at the same volume as during photosynthesis measurements. The light field over the back glass appeared to be homogeneous, and the average light intensity ($q_{exitave}$, Fig. 2) was the same as the light intensity at the center of the glass (q_{exit}), which was monitored during photosynthesis measurements. Using the transmittance of the glass (τ_g, 0.98) reported by the manufacturer, the outgoing light intensity at the liquid side of the back glass (q_{out}) can be obtained:

$$q_{out} = \frac{q_{exitave}}{\tau_g} = \frac{q_{exit}}{\tau_g} \tag{5}$$

2.4.3. Light absorption by algae samples

Almost half of the light entering the chamber was found to be lost in the chamber. It is suspected that part of the light is lost by light absorption on the sidewall of the chamber due to the isotropic character of the incoming light. In this research, the following model was introduced to extract light absorption purely by algae from the whole light attenuation in the chamber.

The light transmittance (τ) was introduced as below:

$$\tau = \frac{q_{out}}{q_{in}} \tag{6}$$

The transmittance when the chamber was filled only with water (τ_w) was calculated by using Eqs. (5) and (6) as below:

$$\tau_w = \frac{q_{out}}{q_{in}} = \frac{q_{exit}}{q_{in} \bullet \tau_g} (= 0.53) \tag{7}$$

The extinction coefficient with water (ε_w) was introduced based on the transmittance with water (τ_w) and the Lamber-Beer law, using the optical path length of the chamber (d). Similarly, the extinction coefficient with algal sample (ε_s) was introduced based on the transmittance with algal sample (τ_s):

$$\varepsilon_w = \frac{-Ln(\tau_w)}{d} \Longleftrightarrow \tau_w = e^{-\varepsilon_w \bullet d} \tag{8}$$

$$\varepsilon_s = \frac{-Ln(\tau_s)}{d} \Longleftrightarrow \tau_s = e^{-\varepsilon_s \bullet d} \tag{9}$$

By introducing the extinction coefficient attributed to light attenuation purely caused by algae (ε_a), the transmittance with algal sample (τ_s) can also be calculated as below. Therefore, the extinction coefficient purely attributed to algae (ε_a) was calculated as below:

$$\tau_s = e^{-(\varepsilon_w + \varepsilon_a) \bullet d} \tag{10}$$

$$\varepsilon_a = \varepsilon_s - \varepsilon_w \tag{11}$$

With Eqs. (9) and (11), the average light intensity in the algal sample (q_{ave}) and the light absorption by algae (q_{abs}) was calculated along the light path (z : 0 mm → d) as below:

$$q_{ave} = \frac{1}{d} \bullet \int_0^d q_{in} \bullet e^{-\varepsilon_s \bullet z} dz = \frac{q_{in}}{\varepsilon_s \bullet d} \bullet (1 - \tau_s) \quad (12)$$

$$q_{abs} = \int_0^d \varepsilon_a \bullet q_{in} \bullet e^{-\varepsilon_s \bullet z} dz = \frac{\varepsilon_a}{\varepsilon_w + \varepsilon_a} \bullet q_{in} \bullet (1 - \tau_s) \quad (13)$$

2.4.4. Biomass yield on light energy ($Y_{x/ph}$)

The biomass yield on light during the light response measurements was calculated as follows:

$$Y_{x/ph} = \frac{A_{CO_2}}{q_{abs}} \bullet M_x \quad (14)$$

where M_x is the molecular weight of biomass, assumed to be 24 g mol^{-1} [46].

To compare with the undiluted samples, the biomass yield on light in the photobioreactor where biomass was cultivated was calculated as below.

$$Y_{x/ph(photobioreactor)} = \frac{P_{x,a}}{I_{abs}} \quad (15)$$

where $P_{x,\,a}$ is the areal biomass productivity in the photobioreactor [g m^{-2} d^{-1}] and I_{abs} is the light absorption by algae in the photobioreactor [mol$_{ph}$ m^{-2} d^{-1}].

The areal biomass productivity ($P_{x,\,a}$) was calculated as follows:

$$P_{x,a} = D_L \bullet C_{x,DW} \bullet 10^3 \bullet d_R \quad (16)$$

where D_L is the dilution rate in the photobioreactor [d^{-1}], $C_{x,\,DW}$ is the biomass concentration based on dry weight measurements [g L^{-1}], and d_R is the optical path in the photobioreactor (0.014 m).

Determination of the volumetric CO_2 gas-liquid mass transfer coefficient ($k_{lCO_2}a$).

The CO_2 concentration in the liquid not only depends on the CO_2 concentration in the gas phase used to sparge the culture, but it also depends on the mass transfer rate over the gas-liquid interface and the CO_2 consumption rate of the microalgae. Considering the accumulation of CO_2 into the liquid phase is null in a steady-state, the CO_2 concentration in liquid (C_{lCO_2}) is calculated as follows:

$$C_{lCO_2} = C_{lCO_2eq} - \frac{q_{CO_2} \bullet C_x}{k_{lCO_2}a} \quad (17)$$

where C_{lCO_2eq} is the equilibrium CO_2 concentration at the gas-liquid interface.

In the aquatic chamber used for this research, the CO_2 assimilation rate ($q_{CO_2} \bullet C_x$) and the equilibrium CO_2 concentration at a gas-liquid interface (C_{lCO_2eq}) can be calculated from the photosynthesis measurements. The volumetric mass transfer coefficient ($k_{lCO_2}a$) of the aquatic chamber needs to be separately determined. This constant depends on chamber design, gas flow rate, and physical properties of the medium. When physical properties of the medium are constant, the gas flow rate determines the volumetric mass transfer coefficient ($k_{lCO_2}a$) in the aquatic chamber, which does not have any other means of mixing other than gas sparging.

The following describes a method to determine the volumetric mass transfer coefficient ($k_{lCO_2}a$) in the aquatic chamber using the capability of the LI-6800 to monitor the pH in the liquid as well as the CO_2 gas concentrations (C_{gCO_2ref} and C_{gCO_2sam}) and the CO_2 exchange flux between gas and liquid (F_{CO_2}). This method makes use of the dynamic response of the carbonate chemistry in a liquid phase following a perturbation in the CO_2 concentration in the gas supplied to the chamber (C_{gCO_2ref}).

$$CO_2(l) + H_2O \rightleftarrows H_2CO_3 \rightleftarrows HCO_3^- + H^+ \quad (18)$$

$$HCO_3^- \rightleftarrows CO_3^{2-} + H^+ \quad (19)$$

An intermediate product, carbonic acid, exists in the first equilibrium, as illustrated in Eq. (18). The formation of carbonic acid (i.e., the hydration of CO_2) could be limiting due to its slow reaction rate. For this reason, carbonic anhydrase was added in this method to catalyze a fast CO_2 hydration reaction such that its kinetics would not interfere with the $k_{lCO_2}a$ determination measurement. Also, carbonic anhydrase is applied in the actual CO_2 response measurement discussed later.

The acid dissociation constant (K_a, calculated in Appendix 3) and its negative logarithm with base 10 (pK_a) for the equilibrium Eqs. (18) and (19) are described in Eqs. (20) and (21), and Eqs. (22) and (23), respectively.

$$K_{a1} = \frac{C_{HCO_3} \bullet C_H}{C_{lCO_2}} \quad (20)$$

$$pK_{a1} = -log_{10}K_{a1} \quad (21)$$

$$K_{a2} = \frac{C_{CO_3} \bullet C_H}{C_{HCO_3}} \quad (22)$$

$$pK_{a2} = -log_{10}K_{a2} \quad (23)$$

where C_{HCO_3}, C_{CO_3}, and C_H are the bicarbonate ion concentration, the carbonate ion concentration, and the hydrogen ion concentration, respectively.

The protocol starts with injecting an aqueous solution of sodium bicarbonate and sodium carbonate into the aquatic chamber, where no CO_2 is supplied. An aqueous solution with sodium bicarbonate (4.2 mM $NaHCO_3$) and sodium carbonate (4.2 mM Na_2CO_3) was prepared with ultra-pure water. These salts were first dried in a desiccator filled with nitrogen gas for 24 h. 15 mL of this solution with 1 mg of carbonic anhydrase (from bovine erythrocytes, MP Biomedicals) was injected into the aquatic chamber and sparged with air stripped of CO_2. Immediately after sample injection, the CO_2 concentration at the inlet to the gas exchange system (C_{gCO_2ref}) was switched from 0 to 2700 μmol mol^{-1}. The other parameters, such as the gas flow rate to the gas exchange system (F_g), the gas flow rate supplied to the aquatic chamber (F_{gcha}), and the chamber temperature, were maintained at the same values as applied during the light response measurements and the carbon response measurements.

When the CO_2 supply to the chamber starts, the added CO_2 brings down the pH in the chamber, which changes the carbonate chemistry as described in Eqs. (18) and (19). The concentration for each carbonate species in liquid (C_{lCO_2}, C_{HCO_3}, C_{CO_3}) changes with time according to the following four balance equations (Eqs. (24) to (27)). We took material exchanges in the two different system compartments into account, assuming an ideal mixing in the gas mixer for gas-gas exchange and the aquatic chamber for gas-liquid exchange (Fig. 1).

Mass balance 1: Gas mixer

$$F_g \bullet \left(C_{gCO_2ref}(t) - C_{gCO_2sam}(t)\right) = F_{gcha} \bullet \left(C_{gCO_2sam}(t) - C_{gCO_2cha}(t)\right) \quad (24)$$

Mass balance 2: Gas phase in the aquatic chamber

$$F_{gcha} \bullet \left(C_{gCO_2sam}(t) - C_{gCO_2cha}(t)\right) = k_{lCO_2}a \bullet \left(C_{lCO_2eq}(t) - C_{lCO_2}(t)\right) \bullet V_{lcha} \quad (25)$$

Mass balance 3: Liquid phase in the aquatic chamber

$$k_{lCO_2}a \bullet \left(C_{lCO_2eq}(t) - C_{l.CO_2}(t)\right) \bullet V_{lcha} = \frac{d}{dt}\left(C_{lCO_2}(t) + C_{HCO_3}(t) + C_{CO3}(t)\right) \bullet V_{lcha} \quad (26)$$

Charge balance:

$$C_{Na} + C_H(t) = C_{OH}(t) + C_{HCO_3}(t) + 2 \bullet C_{CO_3}(t) \quad (27)$$

where C_{gCO_2cha} is the CO_2 concentration at the outlet gas from the

chamber, C_{Na} is the sodium ion concentration, C_{OH} is the hydroxide ion concentration, and V_{lcha} is the liquid volume in the chamber.

C_H was based on the measured pH of the liquid sample, and C_{lCO_2eq} was calculated using measured gas CO_2 concentrations at the outlet of the chamber (C_{gCO_2cha}) as described in Appendix 5. Eq. (24) provides the solution for C_{gCO_2cha}, and Eq. (27) together with the equilibrium constant for water ($K_w = C_H \bullet C_{OH}$) gives the solution for C_{lCO_2}. In addition, substituting Eqs. (20) and (22) into Eq. (25) gives the solution for $k_{lCO_2}a$ as below.

$$C_{gCO_2cha}(t) = C_{gCO_2sam}(t) - \frac{F_g}{F_{gcha}} \bullet \left(C_{gCO_2ref}(t) - C_{gCO_2sam}(t)\right) \tag{28}$$

$$C_{lCO_2}(t) = \frac{C_{Na} + C_H(t) - \frac{K_w}{C_H(t)}}{\frac{K_{a1}}{C_H(t)} + 2 \bullet \frac{K_{a1}}{C_H(t)} \bullet \frac{K_{a2}}{C_H(t)}} \tag{29}$$

$$k_{lCO_2}a = \frac{C_{gCO_2sam}(t) - C_{gCO_2cha}(t)}{C_{lCO_2eq}(t) - C_{lCO_2}(t)} \bullet \frac{F_{gcha}}{V_{lcha}} \tag{30}$$

3. Results & discussions

3.1. Light response curve at high and low biomass concentrations

Light response curves can be measured at different biomass concentrations. A high biomass concentration results in a light response curve representing the response of a dense algal culture in a photobioreactor exposed to a range of light intensities. The light response curve of undiluted samples is depicted in Fig. 3 **(a)**. The photosynthesis rate is represented by the areal CO_2 assimilation rate (A_{CO_2}) as a function of light absorption by algae (q_{abs}).

The light response curve at all the examined light intensities for the undiluted samples is shown in Fig. 3 **(a)**. As the shape of the curve indicates, the photosynthesis rate of the undiluted sample was not saturated even at the maximum light absorption (2210 ± 3 $\mu mol_{ph}\ m^{-2}\ s^{-1}$). The shading effect at high biomass concentrations explains the fact that photosynthesis was not saturated even at high light intensities. At high biomass concentrations, a strong light gradient develops with both a light-saturated zone and a light-limited zone. Increasing light intensities accordingly results in an increase in the light-saturated zone, enhancing the photosynthesis rate.

As for the biomass yield on light energy (i.e., $Y_{x/ph}$), the estimated yield in the light response measurement showed the maximum value of 0.94 $g_x\ mol_{ph}^{-1}$ at 737 $\mu mol_{ph}\ m^{-2}\ s^{-1}$ and gradually decreased up to 0.62 $g_x\ mol_{ph}^{-1}$ at 2210 $\mu mol_{ph}\ m^{-2}\ s^{-1}$. Comparing the biomass yield on light in the photobioreactor where biomass samples were cultivated (refer to the triangle symbol in Fig. 3 **(a)**), the measured yield in the photobioreactor (0.95 ± 0.13 $g_x\ mol_{ph}^{-1}$) resembled the estimated yield from the light response measurement at the light absorption levels nearby the light absorption in the reactor (i.e., 885 $\mu mol_{ph}\ m^{-2}\ s^{-1}$). Besides, at another light absorption level (1473 $\mu mol_{ph}\ m^{-2}\ s^{-1}$), the yield estimated from the light response measurement (0.75 $g_x\ mol_{ph}^{-1}$) was also comparable to the measured yield (0.86 $g_x\ mol_{ph}^{-1}$) in another study where the same algal strain was cultivated in the same type of flat panel photobioreactor [44]. Therefore, a light response measurement with an undiluted sample using the approach in this study would be potentially useful in estimating the photosynthetic response, including the photosynthetic efficiency, in a photobioreactor at different light intensities.

When it comes to the diluted samples (i.e., around 20 times lower concentrations than undiluted samples, Fig. 3 **(b)**), the shape of the light response curve was different from the one in the undiluted samples. In contrast to the one in the undiluted sample, the light response curve in the diluted samples was almost saturated at 913 $\mu mol_{ph}\ m^{-2}\ s^{-1}$: the photosynthesis rate at this light absorption level was already 93 % of the rate at the highest examined light absorption (i.e., 2210 ± 3 $\mu mol_{ph}\ m^{-2}\ s^{-1}$). As with the undiluted samples, the shading effect can explain the observed saturation of photosynthesis in the diluted samples. At low biomass concentrations, increasing light intensities rapidly expands a light-saturated zone because of a weak light gradient. Therefore, at low biomass concentrations, complete saturation of photosynthesis is observed at lower light intensities.

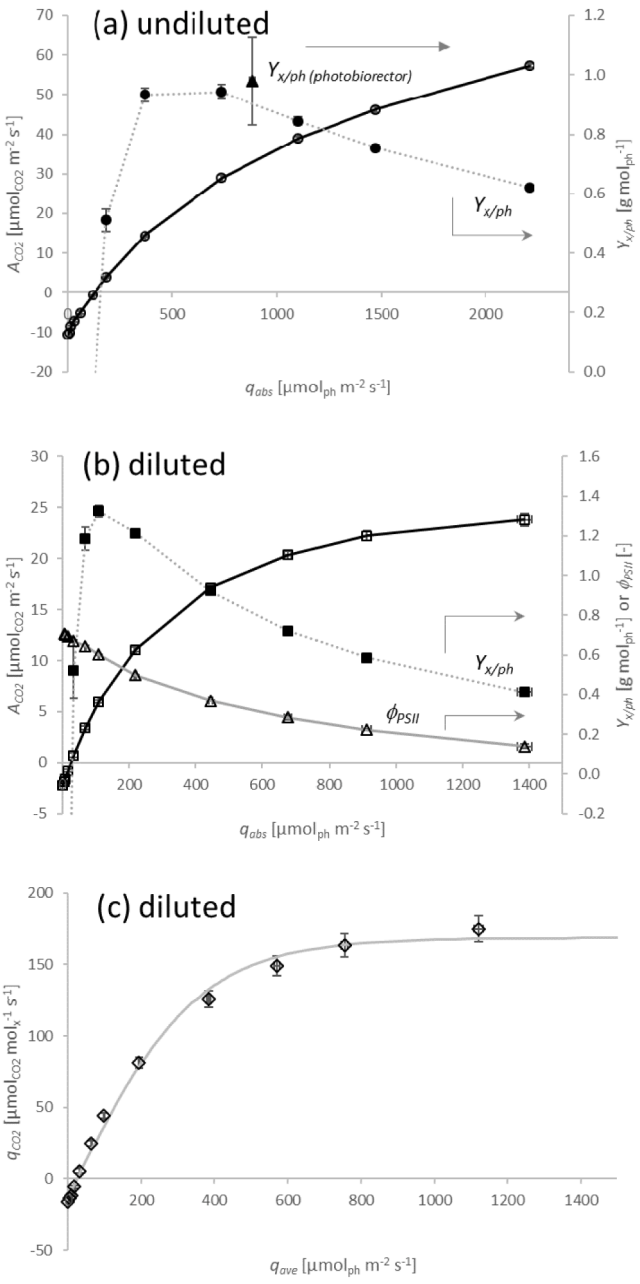

Fig. 3. The light response curve for undiluted samples (a) and diluted samples (b and c): For (a) and (b), the photosynthesis rate is represented by the areal CO_2 assimilation rate (A_{CO_2}) as a function of the light absorption by algae (q_{abs}). For (c), the photosynthesis rate is represented by the specific CO_2 assimilation rate (q_{CO_2}) as a function of the average light intensity (q_{ave}). Error bars represent the standard deviation of biological triplicates.
(a) Undiluted samples at all the examined light intensities (○) shown with the estimated biomass yield on light during light response measurements (● with a grey dotted line) and the measured biomass yield on light in the flat panel photobioreactor where the measured biomass was cultivated (▲). **(b)** Diluted samples at all the examined light intensities (□) shown with the estimated biomass yield on light (■ with a grey dotted line) and measured quantum yield of linear electron transport through PS II (i.e., ϕ_{PSII}, △ with a grey line) during light response measurements. **(c)** Diluted samples: measured light responses (◇) with the fitted hyperbolic tangent model (a grey line).

Turning to the biomass yield on light energy, the change in the yield for the diluted samples with increasing light intensity (i.e., $Y_{x/ph}$ in Fig. 3 **(b)**) also clearly differed from the one for the undiluted samples. Compared with the undiluted samples, the change in the yield for the diluted samples was more drastic, such that a higher maximum yield was obtained at a lower light absorption level: i.e., 1.32 $g_x\ mol_{ph}^{-1}$ at 109 $\mu mol_{ph}\ m^{-2}\ s^{-1}$ in the diluted samples; 0.94 $g_x\ mol_{ph}^{-1}$ at 737 $\mu mol_{ph}\ m^{-2}\ s^{-1}$ in the undiluted samples. After reaching the maximum, the yield rapidly dropped to 0.41 $g_x\ mol_{ph}^{-1}$ at 1386 $\mu mol_{ph}\ m^{-2}\ s^{-1}$.

This observed difference in the photosynthetic efficiency associated with biomass concentrations is reasonable. In dilute cultures, photosynthetic efficiency is higher than in dense cultures at low light intensities because of the lower respiration rate. At following high light intensities, photosynthetic efficiency in dilute cultures more drastically decreases as a light-saturated zone quickly expands with increasing light intensity because of a weak light gradient. This rapid expansion of the light-saturated zone can also be confirmed by a sharp decrease in the quantum yield of the linear electron transport through the photosystem (PS) II (ϕ_{PSII}). ϕ_{PSII} is a measure of the PSII operating efficiency and calculated from the maximal fluorescence in light (F_m') and the fluorescence emission in light (F') as follows: $\phi_{PSII} = (F_m' - F')/F_m'$ [47]. The ϕ_{PSII} was 0.60 at the light absorption when the biomass yield on light was the maximum and dropped to 0.14 at 1386 $\mu mol_{ph}\ m^{-2}\ s^{-1}$ (Fig. 3 **(b)**).

A light response curve must be carried out at low biomass concentrations to extract the light response of individual cells resulting in a biomass specific rate of photosynthesis. In Fig. 3 **(c)**, the specific photosynthesis rate (q_{CO_2}) of the diluted sample is presented as a function of the average light intensity (q_{ave}). The average light intensity was used because even at low biomass density a light gradient develops over the optical path. The hyperbolic tangent model presented in Appendix 2 [48] described the measured light response well, resulting in the following fitting parameters: $q_{CO_2max} = 181.3\ \mu mol_{CO2}\ mol_x^{-1}\ s^{-1}$, $\alpha = 0.519\ mol_{CO2}\ mol_x^{-1}\ mol_{ph}^{-1}\ m^2$, and $R_d = 12.7\ \mu mol_{CO2}\ mol_x^{-1}\ s^{-1}$.

The maximal net specific CO_2 uptake rate of 169 $\mu mol_{CO2}\ mol_x^{-1}\ s^{-1}$ ($q_{CO_2max} - R_d$) we measured is very high compared to the maximal specific growth rate of *Chlorella sorokiniana*. Based on a literature review and model calibration, Blanken et al. [46] estimated the maximal specific growth of *C. sorokiniana* rate at 0.27 h^{-1}. This specific growth rate translates into a net specific CO_2 uptake rate of 75 $\mu mol_{CO2}\ mol_x^{-1}\ s^{-1}$. It appears, therefore, that the photosynthetic capacity of *C. sorokiniana* in the short term exceeds the long-term rate required for biomass growth by far. We hypothesize that carbohydrates (i.e., starch) are rapidly accumulated under this regime of increasing light levels (see light response protocol), mitigating growth limitation downstream of carbon fixation. In the situation of solely starch accumulation, the correction of our rate measurement with the stoichiometric growth coefficient on CO_2 for urea (1/0.93) is not required resulting in a 7 % reduction of our calculated rates. Clearly, such a temporal variation in photosynthetic rate must be further explored. The high photosynthetic rate observed in the light response measurement shows, however, that the applied 2700 ppm of CO_2 in the gas phase (i.e., instrument maximal) is not limiting photosynthesis yet, which makes it a good starting point for the carbon response measurements.

The above-observed differences in light responses between undiluted and diluted cultures clearly highlight the influence of biomass concentration on the photosynthetic light response. Béchet et al. stressed the importance of biomass concentration (or light gradient) in reviewing over 40 studies on mathematical models describing light-limited algal growth and highlighted that most of them overlooked this point during model validation [49]. Our results revealed experimentally and specifically the significance of biomass concentration as follows. Dense cultures show less drastic photosynthetic responses to light intensities because of a high respiration rate and a strong light gradient associated with a high biomass concentration. Besides, a biomass concentration to be used for light response measurement must be carefully chosen depending on the purpose of the measurement. If you want to estimate a photosynthesis rate or a photosynthetic efficiency when changing light intensity in a photobioreactor, you must choose the product of biomass concentration and optical path as close as possible to the one in the photobioreactor. In contrast, you must use a diluted culture if you want to extract the light response of individual cells. In diluted cultures, we observed significantly higher specific photosynthesis rates than estimated rates from a growth rate measured in dense cultivation. A low biomass concentration and a minimal light gradient is a pre-requisite to extracting true biomass specific photosynthetic rates, which are important for strain characterization and physiological characteristics of individual cells.

3.2. Determination of the volumetric CO_2 gas-liquid mass transfer coefficient ($k_{lCO_2}a$)

The dynamics of the CO_2 concentrations in the gas phase (C_{gCO_2ref}, C_{gCO_2sam}, and C_{gCO_2cha}) and the pH after the perturbation to extract the gas liquid transfer coefficient for CO_2 are shown in Fig. 4 **(a)**. The CO_2 concentration at the inlet to the gas mixer (C_{gCO_2ref}) reached the setting value (2700 µmol mol^{-1}) within 1 min after switching the setting value from 0 to 2700 µmol mol^{-1} (t = 0). Soon after (t = 1 min), the CO_2 concentration at the inlet and the outlet of the aquatic chamber (C_{gCO_2sam}

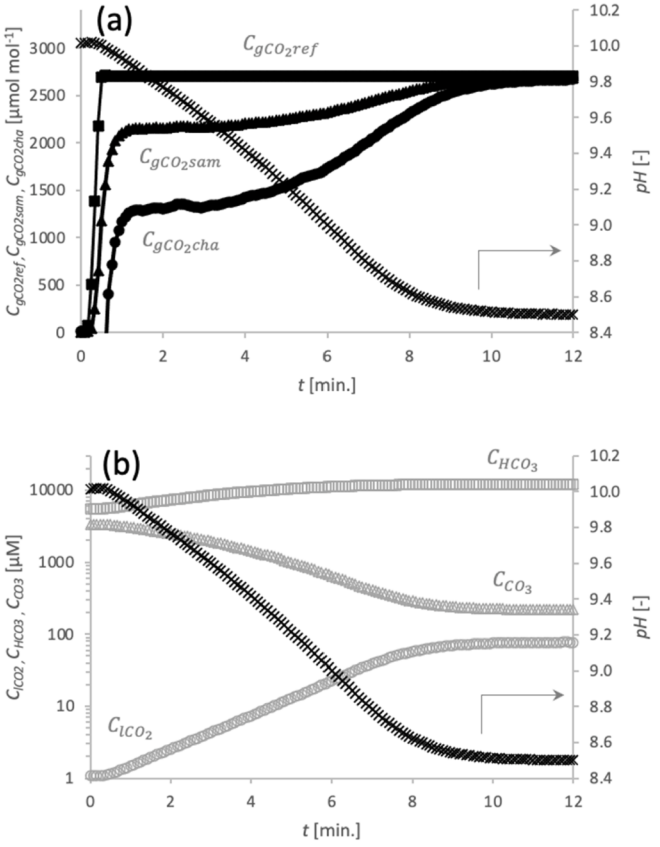

Fig. 4. Dynamic response of CO_2 concentrations in the gas phase and concentrations of carbonate species. **(a)** The CO_2 concentration in the gas phase at different locations and the pH as the function of the time after starting CO_2 supply (t). Squares (■): at the inlet to the gas mixer (C_{gCO_2ref}). Triangles (▲): at the outlet from the aquatic chamber (C_{gCO_2cha}). Circles (●): at the outlet from the aquatic chamber (C_{gCO_2cha}). Crosses (×): the pH in the chamber. **(b)** The concentration of different carbon species and the pH as the function of the time after starting CO_2 supply (t). Circles (○): the CO_2 concentration in the liquid phase (C_{lCO_2}). Squares (□): the bicarbonate ion concentration (C_{HCO_3}). Triangles (△): the carbonate ion concentration (C_{CO_3}). Crosses (×): the pH in the chamber.

and C_{gCO_2cha}) rapidly increased to around 2100 μmol mol^{-1} and 1200 μmol mol^{-1}, respectively. Those two concentrations gradually increased while getting closer to the CO_2 concentration at the inlet to the gas mixer (C_{gCO_2ref}) and showed an almost stable value at $t = 10$ min . Since the concentration difference between the inlet and outlet of the aquatic chamber (C_{gCO_2sam} and C_{gCO_2cha}) indicates the degree of the CO_2 transfer in the chamber, the time change in those two CO_2 concentrations explains that the CO_2 transfer to liquid phase became slower with time and almost stopped at $t = 10$ min.

This behavior is in accordance with the change in the pH in the chamber. The change in the pH indicates that the CO_2 transfer to liquid started soon after the start of the CO_2 supply and stopped after about 10 min because the pH started decreasing from 10.0 at 30 s after starting the CO_2 supply and became stable at 8.5 ($t = 10$ min .). In addition, the change in the calculated concentration of each carbonate species shown in Fig. 4 **(b)** describes the dynamic response in the liquid phase. At the start of the CO_2 supply, the bicarbonate ion and the carbonate ion were dominant in the chamber. While the carbonate ion concentration (C_{CO_3}) soon started decreasing according to the decrease in the pH, the CO_2 concentration (C_{lCO_2}) and the bicarbonate ion concentration (C_{HCO_3}) increased with time and became stable at around $t = 10$ min.

The calculated mass transfer coefficient ($k_{lCO_2}a$) at each time is plotted in Fig. 5. The value stabilized between 0.32 and 0.36 s^{-1} 1 min after starting the CO_2 supply, and it started increasing again above around $t = 7$ min . Since the mass transfer coefficient should be inherently constant, the deviation of the calculated value was considered a consequence of a relative increase of measurement noise at the end of the dynamic response. A CO_2 concentration gradient term ($C_{lCO_2eq} - C_{lCO_2}$) is included in the calculation of the $k_{lCO_2}a$ (Eq. (30)). This term could generate a calculation error, especially when the difference is smaller because those two concentrations (C_{lCO_2eq} and C_{lCO_2}) were based on different measurements respectively: the equilibrium CO_2 concentration (C_{lCO_2eq}) was calculated from the gas analysis while the calculation of the CO_2 concentration in liquid (C_{lCO_2}) was based on the pH measurement. Therefore, unlike the center of the stable period, the calculated concentration difference could have deviated from the real value when those two concentrations became comparable to each other at the ending period of the dynamic response.

The mass transfer coefficient ($k_{lCO_2}a$) during photosynthetic measurements in this research was finally determined as the average in the stable period ($t = 2$ to 6 min .) and found to be 0.34 s^{-1}. This is an extremely high mass transfer rate compared to values obtained in different types of photobioreactors: flat-panel [50], raceway pond [51], and bubble columns [52,53]. As a consequence of this high transfer rate, the liquid CO_2 concentration in the aquatic chamber can be rapidly and accurately set by adjusting the gas CO_2 concentration.

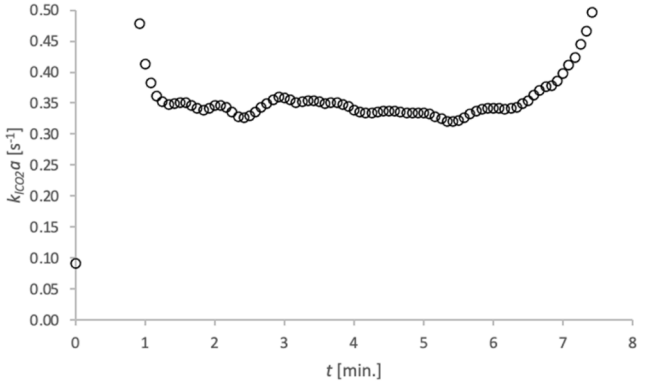

Fig. 5. The calculated mass transfer coefficient ($k_{lCO_2}a$) as a function of the time after starting the CO_2 supply (t).

3.3. Carbon response curve at different oxygen concentrations

The carbon response curves with two different oxygen concentrations (21 % and 2 %) under the ingoing light intensity (q_{in}) of 830 μmol$_{ph}$ m^{-2} s^{-1} are presented in Fig. 6 **(a)**. The curves were drawn as a function of the CO_2 concentration in the liquid phase (C_{lCO_2}). This choice was based on the conclusion by Shelp and Canvin [27] that *Chlorella* uses CO_2 as the main carbon source for photosynthesis, and active uptake of HCO_3^- is minimal at neutral pH. Considering a pH in the range (Table 1) of minimally 7.1 (start experiment) to maximally 7.3 (end experiment), the equilibrium concentration of HCO_3^- is 7.2 to 11.5 fold the CO_2 concentration at 37 °C (Appendix 3 & 4). As shown in the graph, the carbon response curves with both oxygen concentrations showed a similar shape, while the photosynthesis rate under 2 % oxygen concentration was higher at all the CO_2 concentrations except for the condition close to zero. The specific photosynthesis rates sharply increased with the CO_2 concentration up to around 15 μM and then gradually rose in response to the CO_2 concentration.

The photosynthesis rates were not saturated even at the maximum CO_2 concentration in the liquid (65 μM) corresponding to the maximum gas CO_2 concentration (C_{gCO_2ref}, 2700 μmol mol^{-1}) in the measurements.

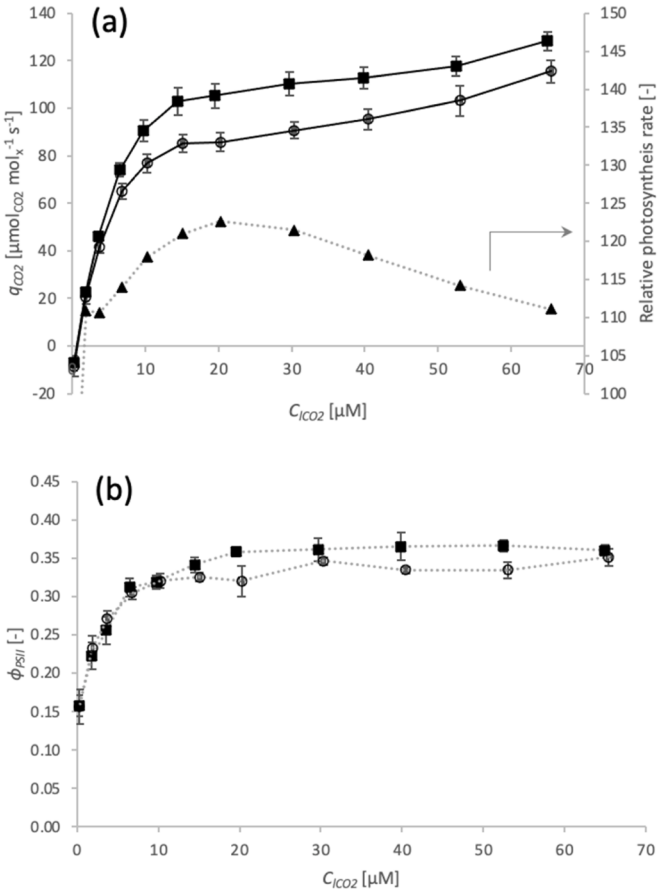

Fig. 6. The carbon response curves at different oxygen concentrations (21 % or 2 % oxygen concentration), $q_{in}$of 830 μmol$_{ph}$ m^{-2} s^{-1} and $q_{ave}$of 380 μmol$_{ph}$ m^{-2} s^{-1}. **(a)** The photosynthesis rate as a function of the CO_2 concentration in the liquid phase (C_{lCO_2}). The photosynthesis was represented by the specific CO_2 assimilation rate (q_{CO_2}). White circles (○): 21 % oxygen. Black squires (■): 2 % oxygen. Black triangles (▲): The relative photosynthesis rate at 2 % oxygen based on the photosynthesis rate at 21 % oxygen. The relative rate of 100 is the photosynthesis rate at each CO_2 concentration under 21 % oxygen. **(b)** The quantum yield of the linear electron transport through PSII (ϕ_{PSII}) as a function of the CO_2 concentration in the liquid phase (C_{lCO_2}). White circles (○): 21 % oxygen. Black squires (■): 2 % oxygen. Error bars represent the standard deviation of biological triplicates.

Photosynthetic response to higher CO_2 concentration was not examined due to the instrument's limitation, and we are unsure if CO_2 uptake would further increase at higher CO_2 levels. Miyauchi et al. [54] also observed such a two-phase increase of photosynthesis as a response to CO_2 concentration for *Chlorella kessleri* biofilms using a CO2-based photosynthesis monitor. These authors were not able to go beyond a CO_2 partial pressure beyond 2000 ppm. Despite this uncertainty, the specific rates measured in our study at 2700 ppm are very high, and we would not expect a large increase at higher CO_2 levels anymore. We found a photosynthesis rate of 116 $\mu mol_{CO2}\ mol_x^{-1}\ s^{-1}$ at 2700 ppm of CO_2 in air and the q_{ave} of 380 $\mu mol_{ph}\ m^{-2}\ s^{-1}$. This rate matches well with the rate measured in the light response cure at equivalent q_{ave} (Fig. 3c). As discussed before, we would expect a photosynthesis rate of 'only' 75 $\mu mol_{CO2}\ mol_x^{-1}\ s^{-1}$ at maximal specific growth of *C. sorokiniana* (0.27 h^{-1}). This comparison illustrates that also, in the short-term carbon response measurement, photosynthesis is significantly higher than during long-term cell growth over several generations.

Photorespiration could explain the difference in the photosynthesis rates at different oxygen concentrations. Fig. 6 **(a)** includes the relative photosynthesis rate at 2 % oxygen concentration based on the photosynthesis rate at 21 % oxygen concentration at each CO_2 concentration. The relative photosynthesis rate showed an11 to 23 % stimulation at 2 % oxygen concentration and a continuous decrease at the CO_2 concentrations above 20 μM. This was not in conjunction with the observation of *Chlorella pyrenoidosa* by Shelp and Canvin [26]. The authors observed only 4 to 5 % stimulation at 2 % oxygen concentration and little dependence of the photosynthesis rate on the CO_2 concentration. They concluded that photorespiration was low or absent in their algal culture. Rotatore and Colman [29] also concluded that photorespiration was absent in their study for *Chlorella ellipsoidea* because kinetic constants for the carboxylation reaction at RuBisCO were not affected by oxygen concentrations. However, our case showed the dependence of the degree of stimulation on CO_2 concentrations (i.e., competitive nature of CO_2 and oxygen). Sforza et al. [55] also found a competitive nature of CO_2 and oxygen in photosynthetic responses for *Chlorella protothecoides* and linked their observation to photorespiration. We assume, from the competitive nature of CO_2 and oxygen, that photorespiration was present in our study and partly regulated the net photosynthesis rate at 21 % oxygen concentration, while the influence was low or absent at 2 % oxygen concentration.

We also examined the hypothesis that the increase of the photosynthesis rate at 2 % oxygen concentration was partly attributed to an enhanced linear electron transport rate. Fig. 6 **(b)** describes the change in the quantum yield of the linear electron transport through the photosystem (PS) II (ϕ_{PSII}), which is a measure of the PSII operating efficiency [47], according to the CO_2 concentration in the liquid. The ϕ_{PSII} at 2 % oxygen concentration was slightly higher (2 to 12 %) at CO_2 concentrations of 15 μM and above. The higher ϕ_{PSII} should have increased the linear electron transport rate, leading to a higher photosynthesis rate, under the assumption that the fraction of light absorbed by PSII over the total light absorption did not change in both oxygen concentrations. However, since the increase in the ϕ_{PSII} was smaller than the increase in the photosynthesis rate observed at reduced oxygen level, enhanced linear electron transport rate cannot fully explain the observations. Moreover, we lack a mechanistic explanation of how a reduction of dissolved oxygen levels could affect linear electron transport.

Continuing on the occurrence of photorespiration, we would expect an increase of photosynthesis for the 2 % treatment in comparison to 21 % *v*/v when moving from high CO_2 concentration (65 μM) to lower levels. This expectation is based on the direct dependence of photorespiration on the ratio of dissolved O_2 over CO_2. Indeed we see an increase from 11 % to 23 % when decreasing CO_2 from 65 μM to 20 μM. However, when moving to even lower CO_2 concentrations, we see the relative increase of photosynthesis at 2 % v/v O_2 decreasing again to 11 %. We hypothesize that this transition is related to the activation of a carbon concentrating mechanism (CCM) at this limiting CO_2 concentration allowing for the active uptake of bicarbonate HCO_3^-. Under these conditions, photosynthesis will be less sensitive to the O_2 concentration as bicarbonate levels are one order of magnitude higher than dissolved CO_2 in the pH range of 7.1 to 7.3 applied during the carbon response measurements.

Microalgae experiencing low CO_2 concentrations have the ability to induce a CCM [22,56]. Rapid induction of a CCM has been reported for several green algae when algal cells were transferred from high CO_2 to low CO_2 concentrations. del Pino Plumed et al. [57] confirmed that *Chlorella pyrenoidosa* started inducing a CCM at the latest 1 h after cells were transferred from 5 % to 300 ppm CO_2 atmosphere. Besides, Palmqvist et al. [56] demonstrated by using fluorescence measurements that *Chlamydomonas reinhardtii* immediately induced a CCM when cells were transferred from 5 % to 100 ppm CO_2 atmosphere. In this study, algal cells cultivated in a CO_2 replete condition were transferred to the photosynthesis monitor. Therefore, a similar rapid induction of a CCM triggered by low dissolved CO_2 concentrations would be expected in this study, considering that 20 μM of dissolved CO_2 was obtained when the CO_2 concentration in the supplied gas was 875 ppm. The activation of a carbon concentrating mechanism could also shed light on the observed two-phase increase of photosynthesis as a response to CO_2 concentration because the transition from the fast to the slow increase also takes place at 20 μM of dissolved CO_2.

3.4. Carbon response curve at different light intensities

Since light and CO_2 are both essential for photosynthesis, a shortage of either raw material will limit photosynthesis. Depending on their relative contribution, which depends on the light intensity and range of CO_2 concentration applied, carbon response curves are characterized by a carbon-limited and a light-limited region. Two different light intensities were applied in our carbon response measurements to investigate the transition point from the carbon-limited region to the light-limited region. The transition point was identified according to the criteria used for leaf photosynthesis described by Sharkey et al. [58]: the carbon-limited region occurs when the photosynthetic (linear) electron transport is increasing along with the CO_2 concentration, and the light-limited region occurs when the photosynthetic electron transport does not change with the CO_2 concentration. The relative electron transport rate (*rETR*) was used for the judgment of the transition. This parameter has been widely used in algal culture studies as a relative measure of the photosynthetic electron transport rate [37,59,60]. The *rETR* in relative units (r.u.) is calculated as the product of the quantum yield of the linear electron transport through PSII (ϕ_{PSII}) and the photon flux density absorbed by algae (q_{abs}).

$$rETR = \phi_{PSII} \bullet q_{abs} \tag{31}$$

The *rETR* as a function of the CO_2 concentration in the liquid (C_{lCO_2}) is shown in Fig. 7 for two different light intensities (q_{in}, 415 and 830 $\mu mol_{ph}\ m^{-2}\ s^{-1}$). At both light intensities, the electron transport rate showed a sharp increase at low CO_2 concentrations, followed by a stabilization of *rETR*. Based on the criteria of Sharkey et al. [58], the transition point was found to be around 7.3 μM at 415 $\mu mol_{ph}\ m^{-2}\ s^{-1}$ and around 10.2 μM at 830 $\mu mol_{ph}\ m^{-2}\ s^{-1}$. A shift of the transition point to higher CO_2 concentration was observed when the light intensity was increased. An overview of the underlying processes of photosynthesis can qualitatively justify this shift in the transition point.

The CO_2 fixation in the Calvin–Benson–Bassham (CBB) cycle is fueled by NADPH and ATP generated by the linear electron transport to regenerate a ribulose-1,5-bisphosphate (RuBP). At low CO_2 concentrations, the linear electron transport rate is lower than the maximally reachable rate determined by the photosynthetic light absorption because the RuBP regeneration rate is limited by the CO_2 concentration (carbon-limited region). However, once the CO_2 concentration reaches the corresponding level to the maximal linear electron transport rate, the photosynthesis switches from the carbon-limited to the light-limited

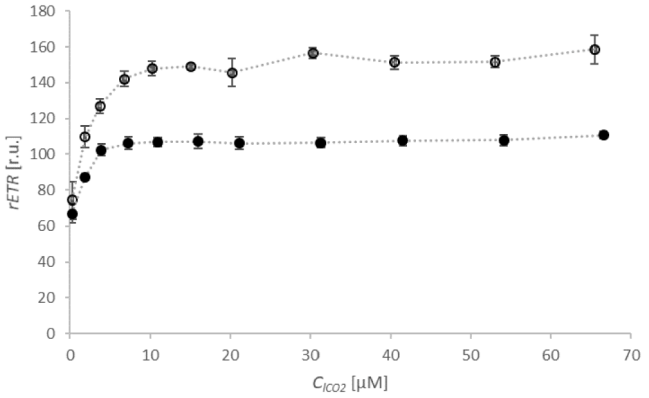

Fig. 7. The carbon response curves at different light intensities. The relative electron transport rate (*rETR*) at different light intensities as a function of the CO_2 concentration in the liquid phase (C_{lCO_2}). White circles (○): 830 $\mu mol_{ph}\ m^{-2}\ s^{-1}$. Black circles (●): 415 $\mu mol_{ph}\ m^{-2}\ s^{-1}$. Error bars represent the standard deviation of biological triplicates.

at this transition point. We explain that in our case the higher light intensity increased the CO_2 concentration corresponding to the maximal linear electron transport rate, which shifted the transition point to the higher concentration.

Future outlook - modeling approach in algal photosynthetic response.

Modeling is a powerful tool as it helps interpret measurement results and predict potential outcomes under given environmental conditions. In leaf photosynthesis, the simple biochemical model describing a photosynthetic CO_2 response in C_3 plants (i.e., the FvCB model) has significantly contributed to understanding the biochemical properties of measured leaves or predicting a photosynthesis rate at certain environmental conditions [15–18]. Therefore, similarly, a valid photosynthetic model is awaited in the algae world, especially with respect to the carbon response of photosynthesis.

In the present study, we applied a new method for quantitative measurement and analysis of suspended algal culture using a CO_2-based photosynthesis monitor. The proposed methodology enables investigating the algal photosynthetic response to CO_2 concentrations, which existing approaches could not fully achieve. Therefore, we consider that the present study would aid in the development of improved algal photosynthesis models by providing an appropriate measurement and analysis approach. Our study highlighted several points that must be taken into account when constructing a valid algal photosynthesis model or using such a model to predict the production of microalgae cultivated in a photobioreactor.

First, the biomass density to be used for photosynthesis rate measurements must be properly selected according to the measurement purpose. As highlighted in our light response measurements (Fig. 3), dense algal culture gives the response to an environmental condition as a mass culture would experience, while a dilute culture provides insights into the photosynthetic response of individual cells. A model based on the former would help predict the production of a photobioreactor under certain environmental conditions. In contrast, a model based on the latter would shed more light on the physiological characteristics of individual microalgal cells.

Second, the status of a CCM during a measurement must be considered when building a photosynthesis model based on a short-term response. The activation of CCM in the middle of measurement was implied in our carbon response measurements at different oxygen concentrations (Fig. 6). An attempt to understand underlying biochemistry from measured data without considering the existence of a CCM would fail by providing inaccurate RuBisCO-related kinetic constants: e.g., an underestimated half-saturation constant for the carboxylation reaction at RuBisCO.

Third, the limiting factor for photosynthesis at each data point must be identified as the underlying biochemistry is different for different limiting factors. In our carbon response measurements at different light intensities (Fig. 7), we showed the transition from the carbon-limited region to the light-limited region at certain CO_2 concentrations and the shift of transition point at different light intensities using simultaneous fluorescence measurements.

Despite the above-mentioned complexities in the algal world, most preceding studies on algal carbon responses just applied the typical Monod's model (Eq. (32)) to all the measured data points to extract kinetic constants without paying attention to the influence of chosen biomass density, the possibility of the existence of a CCM, or the transition from the carbon-limited region to the light-limited region [24,26–30]. This simplification would cause discrepancies from the real behavior of the RuBisCO-involved reactions. Fig. 8 depicts the fitting of the typical Monod's model (Eq. (32)) applied to one of the carbon response curves in this study (i.e., under 830 $\mu mol_{ph}\ m^{-2}\ s^{-1}$ and at 21 % oxygen concentration), resulting in the following fitting parameters: $q_{CO_2max} = 117.1\ \mu mol_{CO2}\ mol_x^{-1}\ s^{-1}$ and $K_{CO_2} = 6.4\ \mu M$.

$$q_{CO_2} = q_{CO_2max} \bullet \frac{C_{lCO_2}}{C_{lCO_2} + K_{CO_2}} \tag{32}$$

where K_{CO_2} is the half-saturation constant for the carboxylation reaction at RuBisCO.

Obviously, the typical Monod model was too simple to describe the carbon response in this study, as shown in Fig. 8. First, the fitted curve did not explain a negative photosynthesis rate observed when the target CO_2 concentration was set at zero. The observed negative photosynthesis rate should be attributed to the light respiration (R_d), which was not incorporated into the Monod model. Second, the fitted curve did not reproduce measured points at all, especially in the light-limited region (i.e., C_{lCO_2} is 15.1 μM or higher). The increase in the measured photosynthesis rate became larger and larger with each increase in the CO_2 concentration, which cannot be described by the Monod model that approaches an asymptote at high CO_2 concentrations. Third, the obtained half-saturation constant for the carboxylation reaction (K_{CO_2}, 6.4 μM) was too low, given that the constant for microalgal RuBisCO is usually on the order of tens μM [61]. This would indicate that CO_2 concentrations at the active site of RuBisCO were elevated from extracellular concentrations. On the one hand, the typical Monod model could still be useful at low CO_2 concentrations for engineering purposes (i.e., prediction of biomass production in a photobioreactor) as it represented our measured data points relatively well in the carbon-limited region. On the other hand, a mathematical equation reflecting complexities described above needs to be developed to accurately understand biological realities behind.

Further investigation should be conducted, especially to verify how

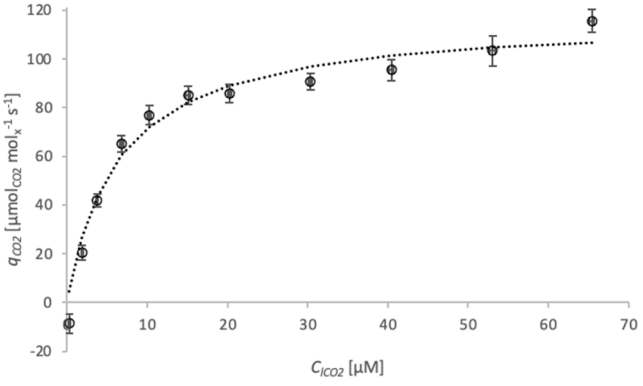

Fig. 8. The fitting of the Monod model: the fitted Monod model (a dotted line) and measured carbon response (○) under 830 $\mu mol_{ph}\ m^{-2}\ s^{-1}$ and at 21 % oxygen concentration.

the impact of a CCM should be incorporated into an algal photosynthesis model. To this end, it would be beneficial to compare the carbon responses of microalgal species or strains expressing and lacking CCM under the same cultivation conditions. Similarly, comparing the carbon response behaviors of the same strain cultivated under CO_2-replete and deplete conditions would also provide new insights for incorporating the effects of a CCM into algal photosynthesis models.

The fitting was applied to the averaged measured points of biological triplicates. The first point (nearby zero CO_2 concentration) was excluded from the fittings because the calculation of CO_2 exchange flux (F_{CO_2}) based on measured CO_2 concentrations close to zero could cause a remarkable error, considering that the accuracy of CO_2 IRGA is ±2 μmol mol^{-1} at CO_2 concentrations below 200 μmol mol^{-1} according to the manufacturer's manual.

4. Conclusions

We investigated the short term light-limited and carbon-limited responses of suspended *Chlorella sorokiniana* using a CO_2-based photosynthesis monitor.. The light response measurements experimentally shed light on the influence of biomass concentrations on photosynthesis. Dense cultures provided a less drastic light response because of higher respiration rates and a strong light gradient associated with higher biomass concentrations. The carbon response measurements at different oxygen concentrations suggested the existence of photorespiration in *Chlorella*. Moreover, the two-phase increase of the photosynthesis rate as a response to CO_2 concentrations indicated the activation of a carbon concentrating mechanism (CCM) along the experimental decrease of dissolved CO_2. Besides, simultaneous fluorescence measurements with CO_2 gas exchange measurements revealed the transition from CO_2-limited to light-limited photosynthesis during the carbon response measurements. This transition of the limiting factor in photosynthesis has not attracted much attention before in algal photosynthetic response measurements. Clearly, the development of improved algal photosynthetic response models must consider the complexities of the algal photosynthetic response described above. The outcomes and methodologies in this study will promote the development of improved algal photosynthetic response models that better describe the reality of the algal world. From an engineering point of view, severe photosynthesis limitation was at dissolved CO_2 concentrations of <20 μM which would be a useful guideline to optimize CO_2 supply in large-scale cultivation systems.

Nomenclature

C_{gCO_2ref}	CO_2 concentration at the inlet of the gas exchange system [μmol mol^{-1}]
C_{gCO_2sam}	CO_2 concentration at the outlet of the gas exchange system [μmol mol^{-1}]
C_{gH_2Oref}	Water vapor concentration at the inlet of the gas exchange system [mmol mol^{-1}]
C_{gH_2Osam}	Water vapor concentration at the outlet of gas exchange system [mmol mol^{-1}]
F_g	Inlet gas flow rate [μmol s^{-1}]
F_{CO_2}	CO_2 exchange flux [μmol s^{-1}]
F_{gcha}	Gas flow rate to aquatic chamber [μmol s^{-1}]
T_{aq}	Temperature of stainless-steel chamber block [°C]
T_{liq}	Liquid temperature [°C]
$k_{lCO_2}a$	Volumetric CO_2 gas-liquid mass transfer coefficient [s^{-1}]
A_{CO_2}	Areal CO_2 assimilation rate [μmol_{CO2} m^{-2} s^{-1}]
q_{CO_2}	Specific CO_2 assimilation rate [μmol_{CO2} mol_x^{-1} s^{-1}]
A_{cham}	Illuminated area in aquatic chamber [m^{-2}] (5.85×10^{-4} m^{-2})
$r_{CO_2/x}$	Stoichiometry of CO_2 to biomass in growth equation [−] (0.93)
C_x	Molar biomass concentration [mol_x m^{-3}]
M_x	Molecular weight of biomass [g mol^{-1}] (24 g mol^{-1} [46])
Q_f	Fluorometer output at the inlet to aquatic chamber [−]
q_{exit}	Light intensity at the outlet from the aquatic chamber [μmol_{ph} m^{-2} s^{-1}]
q_{in}	Incoming light intensity to samples [μmol_{ph} m^{-2} s^{-1}]
q_{out}	Outgoing light intensity from samples [μmol_{ph} m^{-2} s^{-1}]
q_{inave}	Spatial average light intensity over the entire front glass [μmol_{ph} m^{-2} s^{-1}]
f	Conversion factor to estimate q_{in} from Q_f [−]
$q_{exitave}$	Spatial average light intensity over the entire back glass [μmol_{ph} m^{-2} s^{-1}]
τ_g	Light transmittance of glass [−] (0.98)
τ	Light transmittance through samples in aquatic chamber [−]
τ_w	Light transmittance through water in aquatic chamber [−]
ε_w	Extinction coefficient with water in aquatic chamber [m^{-1}]
ε_s	Extinction coefficient with algal samples in aquatic chamber [m^{-1}]
d	Optical path length of the chamber [m] (2.54×10^{-2} (m)
ε_a	Extinction coefficient attributed to light attenuation caused by algae [m^{-1}]
$Y_{x/ph}$	Biomass yield on light energy [g_x mol_{ph}^{-1}]
q_{ave}	Average light intensity in algal sample
q_{abs}	Light absorption by algae
$P_{x,\,a}$	Areal biomass productivity in the photobioreactor [g m^{-2} d^{-1}]
I_{abs}	Light absorption by algae in the photobioreactor [mol_{ph} m^{-2} d^{-1}]
D_L	Dilution rate in the photobioreactor [d^{-1}]
$C_{x,\,DW}$	Biomass concentration in the photobioreactor [g L^{-1}]
d_R	Optical path in the photobioreactor [m]
α	Initial slope of light response curve [mol_{CO2} mol_x^{-1} mol_{ph}^{-1} m^2]
q_{CO_2max}	Maximal specific CO_2 assimilation rate [μmol_{CO2} mol_x^{-1} s^{-1}]
R_d	Day respiration rate [μmol_{CO2} mol_x^{-1} s^{-1}]
C_{lCO_2}	CO_2 concentration in liquid phase of aquatic chamber [μM]
C_{lCO_2eq}	Equilibrium CO_2 concentration at gas-liquid interface in chamber [μM]
H_{CO_2}	Henry constant for CO_2 [Pa m^3 mol_{CO2}^{-1}] (3924 Pa $m_{H_2O}^3$ $mol_{CO_2}^{-1}$ at 37 °C)
K_{a1}	Acid dissociation constant of dissolved CO_2 [M] (4.92×10^{-7} M at 37 °C)
K_{a2}	Acid dissociation constant of bicarbonate ion [M] (5.76×10^{-11} M at 37 °C)
C_{HCO_3}	Bicarbonate ion concentration in liquid phase of aquatic chamber [μM]
C_{CO_3}	Carbonate ion concentration in liquid phase of aquatic chamber [μM]
C_H	Hydrogen ion concentration in liquid phase of aquatic chamber [μM]
C_{gCO_2cha}	CO_2 concentrations at the outlet gas from the chamber [μmol mol^{-1}]
C_{Na}	Sodium ion concentration in liquid phase of aquatic chamber [μM]
C_{OH}	Hydroxide ion concentration in liquid phase of aquatic chamber [μM]
V_{lcha}	Liquid volume in the chamber [mL]
t	Time after starting CO_2 supply in $k_{lCO_2}a$ determination experiment [minutes]
K_w	Ionization constant for water [M^2] (2.4×10^{-14} M^2, [65])
ϕ_{PSII}	Quantum yield of linear electron transport through PS II [−]
F_m'	Maximal fluorescence in light [−]
F'	Fluorescence emission in light [−]
$rETR$	Relative electron transport rate [relative units (r.u.)]
K_{CO_2}	Half-saturation constant for carboxylation reaction at RuBisCO [μM]
Γ	CO_2 compensation point in the presence of day respiration [μM]
P_{cha}	Gas pressure in the aquatic chamber [Pa] (101,525 Pa)

CRediT authorship contribution statement

Hiroki Yoshida: Methodology, Investigation, Formal analysis, Visualization, Writing – original draft, Writing – review & editing. **Sabine van Oossanen:** Supervision, Writing – review & editing. **Maria J. Barbosa:** Resources, Writing – review & editing. **Marcel Janssen:** Conceptualization, Methodology, Supervision, Writing – review & editing.

Declaration of competing interest

The authors declare that they have no known competing financial interests or personal relationships that could have appeared to influence the work reported in this paper.

Data availability

Data will be made available on request.

Acknowledgements

The authors would like to thank LI-COR Biosciences for providing us with access to their aquatic chamber 6800-18 prototype with a CO_2 based photosynthesis monitor LI-6800.

Appendix 1. Growth equation

The elemental composition in the biomass was based on *Chlamydomonas reinhardtii* [62] under the assumption that this composition can be applied to *Chlorella sorokiniana* [44].

$$0.93 \bullet CO_2 + 0.654 \bullet H_2O + 0.011 \bullet H^+ + 0.07 \bullet CH_4ON_2 + 0.011 \bullet H_2PO_4^- \rightarrow CH_{1.62}O_{0.41}N_{0.014}P_{0.011} + 1.109 \bullet O_2 \quad (33)$$

Appendix 2. Jassby and Platt model

The light response curve for the diluted samples was fitted by the following hyperbolic tangent model [48].

$$q_{CO_2} = q_{CO_2max} \bullet tanh\left(\frac{\alpha \bullet q_{ave}}{q_{CO_2max}}\right) - R_d \quad (34)$$

where the initial slope of the curve (α), the maximal specific CO_2 assimilation rate (q_{CO_2max}), and the day respiration rate (R_d, respiration rate in light).

Appendix 3. Acid dissociation constant for dissolved CO2 (K_{a1}) and bicarbonate ion (K_{a2})

The acid dissociation constant for dissolved CO_2 (K_{a1}, Eq. (18)) and bicarbonate ion (K_{a2}, Eq. (19)) were calculated at the liquid temperature (T_{liq}) of 37 °C using the equations on the temperature dependence described by Edwards et al. [63] as follows.

$$lnK_{a1} = \frac{A_1}{T_{liq}[\mathrm{K}]} + B_1 \bullet lnT_{liq}[\mathrm{K}] + C_1 \quad (35)$$

where $A_1 = -12092.1$, $B_1 = -36.7816$, $C_1 = 235.482$.

$$lnK_{a2} = \frac{A_2}{T_{liq}[\mathrm{K}]} + B_2 \bullet lnT_{liq}[\mathrm{K}] + C_2 \quad (36)$$

where $A_2 = -12431.7$, $B_2 = -35.4819$, $C_2 = 220.067$.

K_{a1} and K_{a1} were found to be 4.92×10^{-7} M and 5.76×10^{-11} M, respectively.

Appendix 4. Henry constant for CO_2 (H_{CO_2})

The Henry constant for CO_2 (H_{CO_2}) at the liquid temperature (T_{liq}) of 37 °C was calculated using the equation on the temperature dependence described by Carroll et al. [64] as follows.

$$lnH_{CO_2}\left[\mathrm{MPa}\left(\mathrm{mol_{CO_2}\ mol_{H_2O}^{-1}}\right)^{-1}\right] = D_1 + \frac{D_2}{T_{liq}[\mathrm{K}]} + \frac{D_3}{\left(T_{liq}[\mathrm{K}]\right)^2} + \frac{D_4}{\left(T_{liq}[\mathrm{K}]\right)^3} \quad (37)$$

where $D_1 = -6.8346$, $D_2 = 1.2817 \times 10^4$, $D_3 = -3.7668 \times 10^6$, $D_4 = 2.997 \times 10^8$.

The unit of the constant was converted as below, and H_{CO_2} at 37 °C was found to be 3924 Pa $m_{H_2O}^3\ mol_{CO_2}^{-1}$.

$$H_{CO_2}\left[\mathrm{Pa\ m_{H_2O}^3\ mol_{CO_2}^{-1}}\right] = \frac{H_{CO_2}\left[\mathrm{MPa}\left(\mathrm{mol_{CO_2}\ mol_{H_2O}^{-1}}\right)^{-1}\right] \bullet 10^6 \bullet MW_{H_2O}}{\rho_{H_2O}} \quad (38)$$

where MW_{H_2O} is the molecular weight of water (18×10^{-3} kg mol^{-1}), and ρ_{H_2O} is the density of liquid water at 37 °C (993.4 kg m^{-3}).

Appendix 5. Equilibrium CO_2 concentration at the gas-liquid interface

The equilibrium CO_2 concentration at the gas-liquid interface in the chamber (C_{lCO_2eq}) was calculated using the gas CO_2 concentrations at the outlet of the chamber (C_{gCO_2cha}) and the Henry constant for CO_2 (H_{CO_2}, described in Appendix 4) as follows.

$$C_{lCO_2eq} = \frac{P_{cha} \bullet C_{gCO_2cha}}{H_{CO_2} \bullet 10^3} \tag{39}$$

where P_{cha} is the gas pressure in the chamber (101,525 Pa).

Appendix 6. Supplementary data

Supplementary data to this article can be found online at https://doi.org/10.1016/j.algal.2022.102934.

References

[1] J.A. Bassham, A.A. Benson, L.D. Kay, A.Z. Harris, A.T. Wilson, M. Calvin, The path of carbon in photosynthesis. XXI. The cyclic regeneration of carbon dioxide acceptor, J. Am. Chem. Soc. 76 (1954) 1760–1770, https://doi.org/10.1021/ja01636a012.

[2] L. Krienitz, V.A.R. Huss, C. Bock, Chlorella: 125 years of the green survivalist, Trends Plant Sci. 20 (2015) 67–69, https://doi.org/10.1016/j.tplants.2014.11.005.

[3] K. Nickelsen, The organism strikes back: chlorella algae and their impact on photosynthesis research, 1920s–1960s, Hist. Philos. Life Sci. 39 (2017) 1–22, https://doi.org/10.1007/s40656-017-0137-2.

[4] B.Y.J.S. Turner, E.G. Brittain, Oxygen as a factor in photosynthesis, Biol. Rev. 37 (1962) 130–170.

[5] R. Emerson, R. Chalmers, C. Cederstrand, Some factors influencing the long-wave limit of photosynthesis, Proc. Natl. Acad. Sci. 43 (1957) 133–143, https://doi.org/10.1073/PNAS.43.1.133.

[6] K. Nickelsen, The maximum quantum yield controversy (1937–1955), in: Explain. Photosynth. Model. Biochem. Mech. 1840-1960, Springer Netherlands, Dordrecht, 2015, pp. 149–199, https://doi.org/10.1007/978-94-017-9582-1_5.

[7] B. Kok, On the interrelation of respiration and photosynthesis in green plants, Biochim. Biophys. Acta 3 (1949) 625–631, https://doi.org/10.1016/0006-3002(49)90136-5.

[8] J. Ruiz, G. Olivieri, J. De Vree, R. Bosma, P. Willems, J.H. Reith, M.H.M. Eppink, D. M.M. Kleinegris, R.H. Wijffels, M.J. Barbosa, Towards industrial products from microalgae, Energy Environ. Sci. 9 (2016) 3036–3043, https://doi.org/10.1039/c6ee01493c.

[9] R.H. Wijffels, O. Kruse, K.J. Hellingwerf, Potential of industrial biotechnology with cyanobacteria and eukaryotic microalgae, Curr. Opin. Biotechnol. 24 (2013) 405–413, https://doi.org/10.1016/j.copbio.2013.04.004.

[10] M.I. Khan, J.H. Shin, J.D. Kim, The promising future of microalgae: current status, challenges, and optimization of a sustainable and renewable industry for biofuels, feed, and other products, Microb. Cell Factories 17 (2018) 1–21, https://doi.org/10.1186/S12934-018-0879-X, 2018 171.

[11] F.C. Rubio, F.G.A. Fernández, J.A.S. Pérez, F.G. Camacho, E.M. Grima, Prediction of dissolved oxygen and carbon dioxide concentration profiles in tubular photobioreactors for microalgal culture, Biotechnol. Bioeng. 62 (1999) 71–86, https://doi.org/10.1002/(SICI)1097-0290(19990105)62:1<71::AID-BIT9>3.0.CO;2-T.

[12] J. Pruvost, B. Le Gouic, J.-F. Cornet, Kinetic modeling of CO 2 biofixation by microalgae and optimization of carbon supply in various photobioreactor technologies, ACS Sustain. Chem. Eng. 10 (2022) 12826–12842, https://doi.org/10.1021/ACSSUSCHEMENG.2C03927.

[13] F.G. Acién, J.M. Fernández, J.J. Magán, E. Molina, Production cost of a real microalgae production plant and strategies to reduce it, Biotechnol. Adv. 30 (2012) 1344–1353, https://doi.org/10.1016/j.biotechadv.2012.02.005.

[14] G.D. Farquhar, S. von Caemmerer, J.A. Berry, A biochemical model of photosynthetic CO2 assimilation in leaves of C3 species, Planta 149 (1980) 78–90, https://doi.org/10.1007/BF00386231.

[15] S.P. Long, P.K. Farage, R.L. Garcia, Measurement of leaf and canopy photosynthetic CO2 exchange in the field, J. Exp. Bot. 47 (1996) 1629–1642, https://doi.org/10.1093/jxb/47.11.1629.

[16] S.P. Long, C.J. Bernacchi, Gas exchange measurements, what can they tell us about the underlying limitations to photosynthesis? Procedures and sources of error, J. Exp. Bot. 54 (2003) 2393–2401, https://doi.org/10.1093/jxb/erg262.

[17] X. Yin, P.C. Struik, C3 and C4 photosynthesis models: an overview from the perspective of crop modelling, NJAS Wagening. J. Life Sci. 57 (2009) 27–38, https://doi.org/10.1016/j.njas.2009.07.001.

[18] S. von Caemmerer, Steady-state models of photosynthesis, Plant Cell Environ. 36 (2013) 1617–1630, https://doi.org/10.1111/pce.12098.

[19] R.G. Jensen, J.T. Bahr, Ribulose 1,5-bisphosphate carboxylase-oxygenase.7636, Annu. Rev. Plant Physiol. 65 (1977) 379–400.

[20] W.L. Ogren, Affixing the O to rubisco: discovering the source of photorespiratory glycolate and its regulation, Photosynth. Res. 76 (2003) 53–63, https://doi.org/10.1023/A:1024913925002.

[21] J.V. Moroney, A. Somanchi, How do algae concentrate CO2 to increase the efficiency of photosynthetic carbon fixation? Plant Physiol. 119 (1999) 9–16, https://doi.org/10.1104/pp.119.1.9.

[22] M.H. Spalding, Microalgal carbon-dioxide-concentrating mechanisms: chlamydomonas inorganic carbon transporters, J. Exp. Bot. (2008) 1463–1473, https://doi.org/10.1093/jxb/erm128. Oxford Academic.

[23] G.D. Farquhar, S. von Caemmerer, J.A. Berry, Models of photosynthesis, Plant Physiol. 125 (2001) 42–45, https://doi.org/10.1104/pp.125.1.42.

[24] J.C. Goldman, D. Jenkins, W.J. Oswald, The kinetics of inorganic carbon limited algal growth, J. Water Pollut. Control Fed. 46 (1974) 2785–2787.

[25] J.R. Coleman, B. Colman, Effect of oxygen and temperature on the efficiency of photosynthetic carbon assimilation in two microscopic algae, Plant Physiol. 65 (1980) 980–983, https://doi.org/10.1104/pp.65.5.980.

[26] B.J. Shelp, D.T. Canvin, Photorespiration and oxygen inhibition of photosynthesis in Chlorella pyrenoidosa, Plant Physiol. 65 (1980) 780–784, https://doi.org/10.1104/pp.65.5.780.

[27] B.J. Shelp, D.T. Canvin, Utilization of exogenous inorganic carbon species in photosynthesis by Chlorella pyrenoidosa, Plant Physiol. 65 (1980) 774–779, https://doi.org/10.1104/pp.65.5.774.

[28] J.C. Goldman, S.J. Graham, Inorganic carbon limitation and chemical composition of two freshwater green microalgae, Appl. Environ. Microbiol. 41 (1981) 60–70, https://doi.org/10.1128/aem.41.1.60-70.1981.

[29] C. Rotatore, B. Colman, The acquisition and accumulation of inorganic carbon by the unicellular green alga Chlorella ellipsoidea, Plant Cell Environ. 14 (1991) 377–382, https://doi.org/10.1111/j.1365-3040.1991.tb00946.x.

[30] G.G. Bozzo, B. Colman, Y. Matsuda, Active transport of CO 2 and bicarbonate is induced in response to external CO 2 concentration in the green alga Chlorella kessleri, J. Exp. Bot. 51 (2000) 1341–1348, https://doi.org/10.1093/jxb/51.349.1341.

[31] M.A. Rodrigues, C.P. Dos Santos, Y. Yoneshigue-Valentin, D. Strbac, D.O. Hall, Photosynthetic light-response curves and photoinhibition of the deep-water Laminaria abyssalis and the intertidal Laminaria digitata (Phaeophyceae), J. Phycol. 36 (2000) 97–106, https://doi.org/10.1046/j.1529-8817.2000.98213.x.

[32] S. Sánchez-Fortún, F. Marvá, A. D'Ors, E. Costas, Inhibition of growth and photosynthesis of selected green microalgae as tools to evaluate toxicity of dodecylethyldimethyl-ammonium bromide, Ecotoxicology 17 (2008) 229–234, https://doi.org/10.1007/s10646-007-0189-2.

[33] R. Sivaramakrishnan, S. Suresh, A. Pugazhendhi, J.Mercy Nisha Pauline, A. Incharoensakdi, Response of Scenedesmus sp. to microwave treatment: enhancement of lipid, exopolysaccharide and biomass production, Bioresour. Technol. 312 (2020), 123562, https://doi.org/10.1016/j.biortech.2020.123562.

[34] V.V. Terentyev, A.K. Shukshina, A.A. Ashikhmin, K.G. Tikhonov, A.V. Shitov, The main structural and functional characteristics of photosystem-II-enriched membranes isolated from wild type and cia3 mutant Chlamydomonas reinhardtii, Life 10 (2020), https://doi.org/10.3390/life10050063.

[35] T.S. Pinto, F.X. Malcata, J.D. Arrabaça, J.M. Silva, R.J. Spreitzer, M.G. Esquível, Rubisco mutants of Chlamydomonas reinhardtii enhance photosynthetic hydrogen production, Appl. Microbiol. Biotechnol. 97 (2013) 5635–5643, https://doi.org/10.1007/s00253-013-4920-z.

[36] B. Tamburic, C.R. Evenhuis, D.J. Suggett, A.W.D. Larkum, J.A. Raven, P.J. Ralph, Gas transfer controls carbon limitation during biomass production by marine microalgae, ChemSusChem 8 (2015) 2727–2736, https://doi.org/10.1002/cssc.201500332.

[37] J.R.F. Malapascua, C.G. Jerez, M. Sergejevová, F.L. Figueroa, J. Masojídek, Photosynthesis monitoring to optimize growth of microalgal mass cultures: application of chlorophyll fluorescence techniques, Aquat. Biol. 22 (2014) 123–140, https://doi.org/10.3354/ab00597.

[38] S. Raso, B. van Genugten, M. Vermuë, R.H. Wijffels, Effect of oxygen concentration on the growth of nannochloropsis sp. At low light intensity, J. Appl. Phycol. 24 (2012) 863–871, https://doi.org/10.1007/s10811-011-9706-z.

[39] C. Sousa, A. Compadre, M.H. Vermuë, R.H. Wijffels, Effect of oxygen at low and high light intensities on the growth of neochloris oleoabundans, Algal Res. 2 (2013) 122–126, https://doi.org/10.1016/j.algal.2013.01.007.

[40] A. Kazbar, G. Cogne, B. Urbain, H. Marec, B. Le-Gouic, J. Tallec, H. Takache, A. Ismail, J. Pruvost, Effect of dissolved oxygen concentration on microalgal

culture in photobioreactors, Algal Res. 39 (2019), 101432, https://doi.org/10.1016/j.algal.2019.101432.
[41] E. Ögren, Convexity of the photosynthetic light-response curve in relation to intensity and direction of light during growth, Plant Physiol. 101 (1993) 1013–1019, https://doi.org/10.1104/pp.101.3.1013.
[42] A. Melis, J. Neidhardt, J.R. Benemann, Dunaliella Salina (Chlorophyta) with small chlorophyll antenna sizes exhibit higher photosynthetic productivities and photon use efficiencies than normally pigmented cells, J. Appl. Phycol. 10 (1998) 515–525, https://doi.org/10.1023/A:1008076231267.
[43] S.M. Rincon, N.F. Urrego, K.J. Avila, H.M. Romero, H. Beyenal, Photosynthetic activity assessment in mixotrophically cultured Chlorella vulgaris biofilms at various developmental stages, Algal Res. 38 (2019), 101408, https://doi.org/10.1016/j.algal.2019.101408.
[44] T. de Mooij, Z.R. Nejad, L. van Buren, R.H. Wijffels, M. Janssen, Effect of photoacclimation on microalgae mass culture productivity, Algal Res. 22 (2017) 56–67, https://doi.org/10.1016/j.algal.2016.12.007.
[45] J. Hupp, J.I.E. McCoy, A.J. Millgan, G. Peers, Simultaneously measuring carbon uptake capacity and chlorophyll a fluorescence dynamics in algae, Algal Res. 58 (2021), 102399, https://doi.org/10.1016/j.algal.2021.102399.
[46] W. Blanken, P.R. Postma, L. de Winter, R.H. Wijffels, M. Janssen, Predicting microalgae growth, Algal Res. 14 (2016) 28–38, https://doi.org/10.1016/j.algal.2015.12.020.
[47] N.R. Baker, Chlorophyll fluorescence: a probe of photosynthesis in vivo, Annu. Rev. Plant Biol. 59 (2008) 89–113, https://doi.org/10.1146/annurev.arplant.59.032607.092759.
[48] A.D. Jassby, T. Platt, Mathematical formulation of the relationship between photosynthesis and light for phytoplankton, Limnol. Oceanogr. 21 (1976) 540–547, https://doi.org/10.4319/lo.1976.21.4.0540.
[49] Q. Béchet, A. Shilton, B. Guieysse, Modeling the effects of light and temperature on algae growth: state of the art and critical assessment for productivity prediction during outdoor cultivation, Biotechnol. Adv. 31 (2013) 1648–1663, https://doi.org/10.1016/j.biotechadv.2013.08.014.
[50] E. Sierra, F.G. Acién, J.M. Fernández, J.L. García, C. González, E. Molina, Characterization of a flat plate photobioreactor for the production of microalgae, Chem. Eng. J. 138 (2008) 136–147, https://doi.org/10.1016/j.cej.2007.06.004.
[51] J.L. Mendoza, M.R. Granados, I. de Godos, F.G. Acién, E. Molina, S. Heaven, C. J. Banks, Oxygen transfer and evolution in microalgal culture in open raceways, Bioresour. Technol. 137 (2013) 188–195, https://doi.org/10.1016/j.biortech.2013.03.127.
[52] O.N. Manjrekar, Y. Sun, L. He, Y.J. Tang, M.P. Dudukovic, Hydrodynamics and mass transfer coefficients in a bubble column photo-bioreactor, Chem. Eng. Sci. 168 (2017) 55–66, https://doi.org/10.1016/j.ces.2017.04.016.
[53] M. Mubarak, A. Shaija, P. Prashanth, Bubble column photobioreactor for Chlorella pyrenoidosa cultivation and validating gas hold up and volumetric mass transfer coefficient, Energy Sources Part A 00 (2019) 1–15, https://doi.org/10.1080/15567036.2019.1680769.
[54] H. Miyauchi, K. Okada, S. Fujiwara, M. Tsuzuki, Characterization of CO2 fixation on algal biofilms with an infrared gas analyzer and importance of a space-rich structure on the surface, Algal Res. 46 (2020), 101814, https://doi.org/10.1016/j.algal.2020.101814.
[55] E. Sforza, M. Pastore, S.M. Franke, E. Barbera, Modeling the oxygen inhibition in microalgae: an experimental approach based on photorespirometry, Nat. Biotechnol. 59 (2020) 26–32, https://doi.org/10.1016/j.nbt.2020.06.003.
[56] K. Palmqvist, L.G. Sundblad, G. Wingsle, G. Samuelsson, Acclimation of photosynthetic light reactions during induction of inorganic carbon accumulation in the green alga Chlamydomonas reinhardtii, Plant Physiol. 94 (1990) 357–366, https://doi.org/10.1104/pp.94.1.357.
[57] M. del Pino Plumed, A. Villarejo, A. De Los Ríos, G. García-Reina, Z. Ramazanov, The CO2-concentrating mechanism in a starchless mutant of the green unicellular alga Chlorella pyrenoidosa, Planta 200 (1996) 28–31, https://doi.org/10.1007/BF00196645.
[58] T.D. Sharkey, C.J. Bernacchi, G.D. Farquhar, E.L. Singsaas, Fitting photosynthetic carbon dioxide response curves for C3 leaves, Plant Cell Environ. 30 (2007) 1035–1040, https://doi.org/10.1111/j.1365-3040.2007.01710.x.
[59] J.W. Hofstraat, J.C.H. Peeters, J.F.H. Snel, C. Geel, Simple determination of photosynthetic efficiency and photoinhibition of Dunaliella tertiolecta by saturating pulse fluorescence measurements, Mar. Ecol. Prog. Ser. 103 (1994) 187–196, https://doi.org/10.3354/meps103187.
[60] S. White, A. Anandraj, F. Bux, PAM fluorometry as a tool to assess microalgal nutrient stress and monitor cellular neutral lipids, Bioresour. Technol. 102 (2011) 1675–1682, https://doi.org/10.1016/j.biortech.2010.09.097.
[61] J. Beardall, J.A. Raven, Structural and biochemical features of carbon acquisition in algae, in: Photosynth. Algae Biochem. Physiol. Mech, Springer, Cham, 2020, pp. 141–160, https://doi.org/10.1007/978-3-030-33397-3_7.
[62] A.M.J. Kliphuis, A.J. Klok, D.E. Martens, P.P. Lamers, M. Janssen, R.H. Wijffels, Metabolic modeling of Chlamydomonas reinhardtii: energy requirements for photoautotrophic growth and maintenance, J. Appl. Phycol. 24 (2012) 253–266, https://doi.org/10.1007/s10811-011-9674-3.
[63] T.J. Edwards, G. Maurer, J. Newman, J.M. Prausnitz, Vapor-liquid equilibria in multicomponent aqueous solutions of volatile weak electrolytes, AIChE J. 24 (1978) 966–976, https://doi.org/10.1002/aic.690240605.
[64] J.J. Carroll, J.D. Slupsky, A.E. Mather, The solubility of carbon dioxide in water at low pressure, J. Phys. Chem. Ref. Data 20 (1991) 1201–1209, https://doi.org/10.1063/1.555900.
[65] W.L. Marshall, E.U. Franck, The IAPWS formulation 1995 for the thermodynamic properties of ordinary water substance for general and scientific use, J. Phys. Chem. Ref. Data 10 (1981) 387, https://doi.org/10.1063/1.555643.